Stem Cell Reports
Article

ISSCR

OPEN ACCESS

Single-cell transcriptome analysis of xenotransplanted human retinal organoids defines two migratory cell populations of nonretinal origin

Ying V. Liu,[1,11] Clayton P. Santiago,[2,11] Akin Sogunro,[3] Gregory J. Konar,[1] Ming-wen Hu,[1] Minda M. McNally,[1] Yu-chen Lu,[1] Miguel Flores-Bellver,[4] Silvia Aparicio-Domingo,[4] Kang V. Li,[4] Zhuo-lin Li,[1] Dzhalal Agakishiev,[1] Sarah E. Hadyniak,[3] Katarzyna A. Hussey,[3] Tyler J. Creamer,[5] Linda D. Orzolek,[5] Derek Teng,[1] M. Valeria Canto-Soler,[4] Jiang Qian,[1] Zheng Jiang,[6] Robert J. Johnston, Jr.,[2,3,*] Seth Blackshaw,[1,2,7,8,9,*] and Mandeep S. Singh[1,10,*]

[1]Wilmer Eye Institute, Johns Hopkins University School of Medicine, Baltimore, MD, USA
[2]Solomon H. Snyder Department of Neuroscience, Johns Hopkins University School of Medicine, Baltimore, MD, USA
[3]Department of Biology, Krieger School of Arts and Sciences, Johns Hopkins University, Baltimore, MD, USA
[4]*CellSight* Ocular Stem Cell and Regeneration Program, Department of Ophthalmology, Sue Anschutz-Rodgers Eye Center, University of Colorado, School of Medicine, Aurora, CO, USA
[5]Institute for Basic Biomedical Sciences, Johns Hopkins University School of Medicine, Baltimore, MD, USA
[6]Department of Ophthalmology, Baylor College of Medicine, Houston, TX, USA
[7]Department of Neurology, Johns Hopkins University School of Medicine, Baltimore, MD, USA
[8]Institute for Cell Engineering, Johns Hopkins University School of Medicine, Baltimore, MD, USA
[9]Kavli Neuroscience Discovery Institute, Johns Hopkins University School of Medicine, Baltimore, MD, USA
[10]Department of Genetic Medicine, Johns Hopkins University School of Medicine, Baltimore, MD, USA
[11]These authors contributed equally
*Correspondence: robertjohnston@jhu.edu (R.J.J.), sethblackshaw@gmail.com (S.B.), singhcorrespauth@gmail.com (M.S.S.)
https://doi.org/10.1016/j.stemcr.2023.04.004

SUMMARY

Human retinal organoid transplantation could potentially be a treatment for degenerative retinal diseases. How the recipient retina regulates the survival, maturation, and proliferation of transplanted organoid cells is unknown. We transplanted human retinal organoid-derived cells into photoreceptor-deficient mice and conducted histology and single-cell RNA sequencing alongside time-matched cultured retinal organoids. Unexpectedly, we observed human cells that migrated into all recipient retinal layers and traveled long distances. Using an unbiased approach, we identified these cells as astrocytes and brain/spinal cord-like neural precursors that were absent or rare in stage-matched cultured organoids. In contrast, retinal progenitor-derived rods and cones remained in the subretinal space, maturing more rapidly than those in the cultured controls. These data suggest that recipient microenvironment promotes the maturation of transplanted photoreceptors while inducing or facilitating the survival of migratory cell populations that are not normally derived from retinal progenitors. These findings have important implications for potential cell-based treatments of retinal diseases.

INTRODUCTION

Transplantation of immature retinal cells, such as photoreceptor precursor cells and retinal progenitor cells, has the potential to restore function to the degenerated or dysfunctional human retina. Vision loss may be retarded or reversed by direct cellular integration or cellular material transfer (Bartsch et al., 2008; Gouras et al., 1994; Kalargyrou et al., 2021; Kwan et al., 1999; Lamba et al., 2009; MacLaren et al., 2006; Ortin-Martinez et al., 2021; Pearson et al., 2012, 2016; Santos-Ferreira et al., 2016; Singh et al., 2013, 2016; Yang et al., 2010). Stem cell-derived retinal organoids (Assawachananont et al., 2014; Capowski et al., 2019; Eiraku et al., 2011; Eldred et al., 2018; Gonzalez-Cordero et al., 2013; Kaewkhaw et al., 2015; Mandai et al., 2017; Nakano et al., 2012; Shirai et al., 2016; Tucker et al., 2013; Wahlin et al., 2017; Zhong et al., 2014) are potential sources of renewable and standardized donor cells for therapy. Successful transplantation of these cells will require more advanced understanding of the interactions between donor cells and the recipient microenvironment. Here we address this challenge by transplanting human retinal organoid-derived donor cells subretinally into recipient mice and examining how the recipient microenvironment affects donor cells.

A substantial body of data in multiple animal models supports the regenerative potential of non-migratory donor photoreceptor precursor-derived cells that mature in the recipient subretinal space, spurring experiments in large animals (Aboualizadeh et al., 2020; Ghosh et al., 2004; Klassen et al., 2007; Shirai et al., 2016; Tu et al., 2019; Zhou et al., 2011) en route to clinical studies (Berger et al., 2003; Das et al., 1999; Humayun et al., 2000; jCyte and California Institute for Regenerative, 2020; Liu et al., 2017; ReNeuron, 2022). Aside from the non-migratory cells, migratory donor cells in the inner retinal layers overlying the graft have been observed (Foik et al., 2018; Hambright et al., 2012; Klassen et al., 2004; Lin et al., 2018; Luo et al., 2014; McLelland et al., 2018; Thomas et al., 2021; Yamasaki et al., 2022; Yang et al., 2002; Zou et al., 2019),

which do not appear to be essential for the therapeutic mechanism. These observations raised concerns that long-range migration of donor cells beyond the graft margins may trigger immune exposure and invasive tissue damage. In the few studies of photoreceptor transplantation in nonhuman primate recipients (Shirai et al., 2016; Tu et al., 2019), migratory cells have occasionally been observed (Tu et al., 2019), raising the possibility that it may also occur in humans. Studying the migration of donor cells may also illuminate strategies to regulate their spatial targeting, as with retinal ganglion cell homing in response to an induced chemokine gradient (Soucy et al., 2021). Here, we assess the effects of the recipient retinal microenvironment on the maturation and migratory behavior of transplanted cells derived from human retinal organoids. We molecularly define the identity of the migratory cells that depart from, and the non-migratory cells that remain in, the subretinal graft.

Whereas cell movement is not readily observed in the normal and pathological adult retina, retinal progenitor cells and their descendants undergo considerable radial migration and limited tangential migration during neurogenesis (Poggi et al., 2005; Turner and Cepko, 1987; Turner et al., 1990). In contrast, other CNS cells, including GABAergic neural precursors in the telencephalon (Park et al., 2002) and optic nerve-derived astrocytes in the retina (Paisley and Kay, 2021), undergo long-distance tangential migration. Similarly, stem cells and their progeny migrate following transplantation into the CNS (Liu et al., 2000; Scheffler et al., 2003; Srivastava et al., 2006; Tabar et al., 2005). Thus, each developmental or transplantation context differentially regulates migration.

The origin, heterogeneity, spatial distribution, and proliferative capacity of migratory donor cells derived from retinal sources have not been characterized. Migratory cells can arise from human retinal organoids (Foik et al., 2018; McLelland et al., 2018; Thomas et al., 2021; Tu et al., 2019; Yamasaki et al., 2022; Zou et al., 2019) and human fetal retina (Lin et al., 2018; Zhou et al., 2015), suggesting that migratory behavior is not unique to donor cells obtained through pluripotent stem cell culture. Migratory donor cells were observed in mouse, rat, cat, and nonhuman primate retinas, and in normal and degenerative retinas (Hambright et al., 2012; Klassen et al., 2004; Luo et al., 2014; McLelland et al., 2018; Singh et al., 2019; Tu et al., 2019; Yang et al., 2002; Zhu et al., 2018), suggesting that this phenomenon is common across recipient species and independent of retinal health. A few migratory cells were reported to express GFAP (Yang et al., 2002; Zhu et al., 2018), progenitor markers (e.g., PAX6, Nestin) (Luo et al., 2014; Zhu et al., 2018) or neuronal markers (e.g., MAP2, β-tubulin3) (Seiler et al., 2014), but not mature photoreceptor markers (Foik et al., 2018; Hambright et al., 2012; McLelland et al., 2018; Seiler et al., 2017; Thomas et al., 2021; Tu et al., 2019; Yamasaki et al., 2022; Zhu et al., 2018; Zou et al., 2019). Gasparini et al., in a study of the influence of the murine retinal microenvironment on the morphological maturation of transplanted donor human cone photoreceptors, also observed migratory cells but did not molecularly characterize these cells (Gasparini et al., 2022). Our studies use an unbiased approach to molecularly characterize the migratory and non-migratory cells that arise from human retinal organoids following transplantation into mice.

To understand how the recipient microenvironment influences donor cells, we transplanted the micro-dissected multilayered retinal fragments from human retinal organoids into mouse retinas and used imaging and single cell transcriptomics to characterize the identities, maturity, and migratory activities of graft-derived cells. We identified donor-derived migratory astrocytes and brain/spinal cord-like neural precursors that do not normally arise from retinal progenitor cells, and found that non-migratory photoreceptors matured more rapidly in the subretinal space. Our findings highlight a key strength of organoid-derived cell transplantation in promoting photoreceptor maturation and a potential weakness in the expansion and widespread tangential migration of a population of migratory astrocytes and brain/spinal cord-like neural precursor cells.

RESULTS

Subretinally transplanted human cells migrate from or remain in the subretinal space

To determine how the recipient subretinal space affects donor cells, we differentiated human retinal organoids, dissected them into retinal fragments and transplanted them into recipient mice, and later assessed donor cell position, fate, and maturity. To generate recipient mice, we crossed and bred mice with immune deficiency and retinal degeneration (Figure S1). These C3H/HeJ-*Pde6b*$^{Rd1/Rd1}$ (*Rd1*) and NOD.Cg-*Prkdc*^{scid}/J (*NOD/Scid*) double mutant mice are termed *Rd1/NS*. To generate donor cells, we used H9 human embryonic stem cells (hESCs) carrying a reporter that is expressed in both rod and cone photoreceptors (CRX:tdTomato) (Phillips et al., 2018). We used a gravity aggregation approach to differentiate stem cells into retinal organoids with robust generation of photoreceptors (Eldred et al., 2018; Nakano et al., 2012; Wahlin et al., 2017). On day 134 of organoid culture, we micro-dissected the human retinal organoids and transplanted the fragments into the subretinal space of recipient eyes (n = 16 eyes). Four and a half months later, we evaluated the transplants.

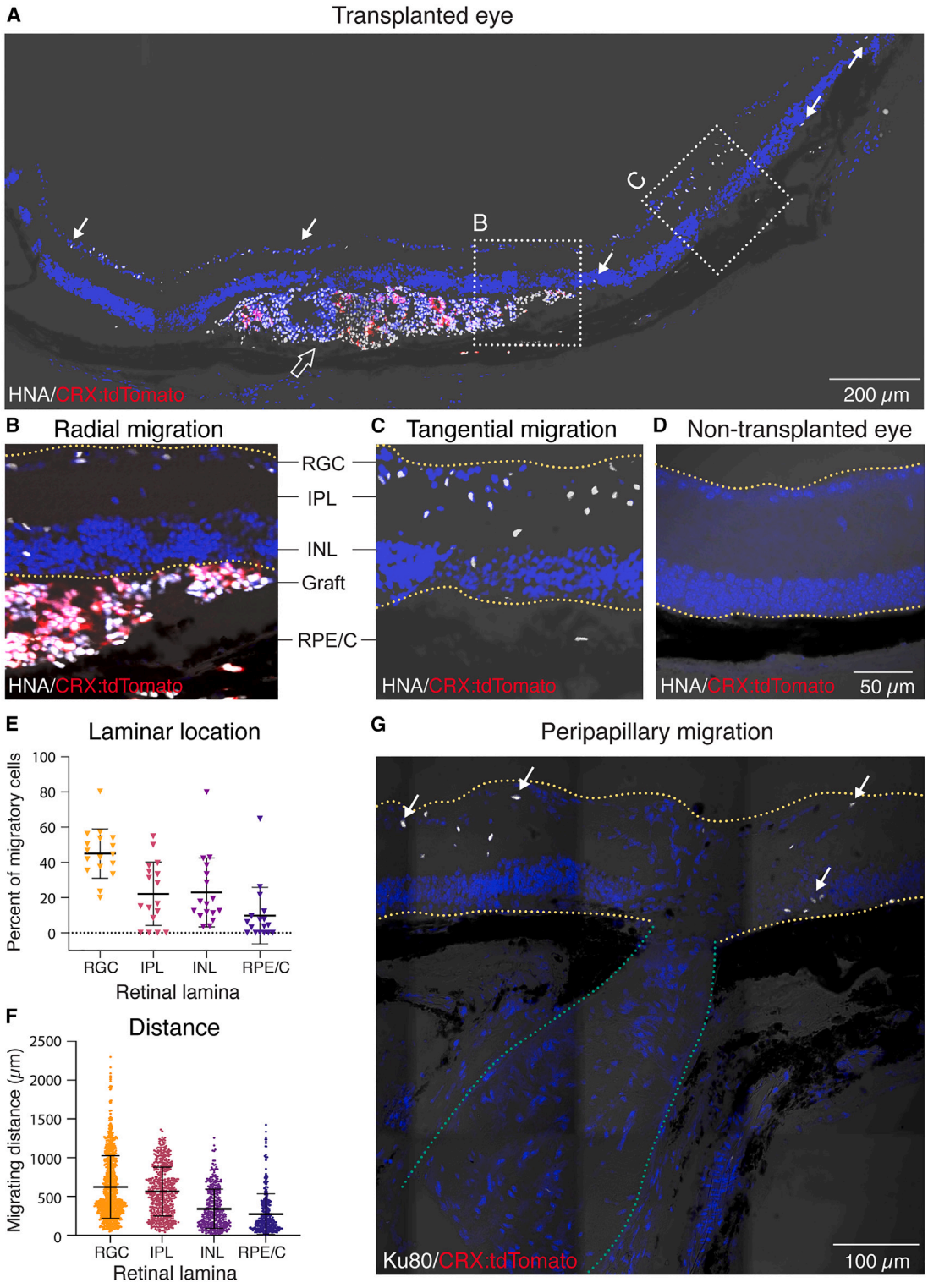

Figure 1. Subretinally transplanted human cells migrate from, or remain in, the subretinal space

(A) IHC staining of human nuclear antigen (HNA) showed migratory (arrows) and non-migratory (empty arrow) human cells in the mouse retina. Transplanted photoreceptors were identified by the expression of CRX:tdTomato reporter.

(B and C) Migratory cells were detected overlying the graft (radial migration) and beyond the graft edge (tangential migration).

(legend continued on next page)

As homozygosity for the *Rd1* allele causes virtually all photoreceptors to degenerate by adulthood in mice (Bowes et al., 1990), distinct recipient outer nuclear and outer plexiform layers were not observed but the inner nuclear, inner plexiform, retinal ganglion cell (RGC), and retinal nerve fiber layers (collectively, the "inner retina") were present.

We determined the positions of donor cells relative to the subretinal transplantation site. We identified all human donor cells on the basis of immunolabeling for human nuclear antigen (HNA) or human ATP-dependent DNA helicase 2 subunit (Ku80 protein). We identified human donor photoreceptors on the basis of transgenic expression of CRX:tdTomato (Figure 1A). We observed two main classes of donor cells: (1) human cells in the recipient subretinal space ("non-migratory cells") that included both photoreceptor or non-photoreceptor cells (Figure 1A) and (2) human cells within the recipient inner retina ("migratory cells") that were not photoreceptors (Figure 1A), suggesting that this population had migrated from the graft. Migratory cells were observed in the recipient inner retinal layers overlying the graft ("radial migration"; Figure 1B), whereas others had migrated away from and beyond the edges of the graft ("tangential migration"; Figure 1C). Migratory cells traveled into all retinal layers, including the retinal ganglion cell layer, inner plexiform layer (IPL), inner nuclear layer (INL), and retinal pigment epithelium/choroid (RPE/C) layer (Figure 1E). Of the tangential migratory cells (n = 2,378 cells), 98.9% were within 1,500 μm of the edges of the graft. The remaining 1.1% traveled beyond 1,500 μm and were located exclusively in the RGC layer (Figure 1F). We detected several migratory human cells in the regions flanking the optic nerve ("peripapillary migration"; Figure 1G) but none in the optic nerve itself. We next sought to molecularly classify the fates of these non-migratory and migratory cells.

Subretinal microenvironment facilitates the proliferation, differentiation and/or survival of retinal and nonretinal cells

To determine how the recipient subretinal microenvironment affects the gene expression and the specification of the migratory and non-migratory donor cells, we conducted single-cell RNA sequencing (scRNA-seq) on cells from human CRX:tdTomato$^+$ retinal organoids transplanted and matured *in vivo* ("transplanted organoids") and from age-matched CRX:tdTomato$^+$ retinal organoids that were maintained *in vitro* ("cultured organoids") (Figure 2A). We analyzed a total of 5,831 human cells that were recovered from the transplanted (1,561 cells) and cultured (4,270 cells) organoids. We identified retinal cell types including retinal progenitor cells (RPCs), photoreceptor precursor cells, rods, cones, bipolar cells, horizontal cells, and Müller glia on the basis of their gene expression profiles (Figures 2B–2D). The quantities of cones, bipolar cells, and horizontal cells were similar in the transplanted and cultured organoids. In contrast, retinal progenitor cells, photoreceptor (PR) precursor cells, and Müller glia were more abundant in cultured organoids, whereas rods were more abundant in transplanted organoids (Figure 2E). The smaller populations of RPCs and photoreceptor precursor cells and larger population of rods in the transplanted organoids suggest that the recipient microenvironment promotes the survival and/or maturation of exogenous photoreceptor cells.

In addition to these cell types, we identified two cell clusters that could not be ascribed solely to known retinal-derived cell fates. The cells in one cluster expressed genes that are broadly expressed in retinal and other CNS progenitors such as *ASCL1* (Figure 2D) and *HES6* (Figure S2). They also expressed genes that are not normally detected in the developing retina including *NKX2-2* and *ARX*, both of which are prominently expressed in telencephalic and/or diencephalic neural progenitors, as well as *HOXC8*, whose expression is normally restricted to the developing spinal cord (Figure 2D). On the basis of this gene expression profile, we designated the cells in this cluster as "brain and spinal cord-like" (BSL) cells. BSL cells comprised approximately 1% of cells in the cultured organoids but were more than 30 times more abundant in the transplanted organoids (Figure 2E). Cells in the second cluster expressed markers characteristic of retinal astrocytes, such as *PAX2* and *S100B* (Figure 2D). Normally, retinal astrocytes are born in the optic nerve head and migrate into the retina. Strikingly, astrocytes were entirely absent in the cultured organoids but constituted approximately 8% of cells in the transplanted organoids (Figure 2E). These data suggest that microenvironmental cues in the host retina allow the proliferation, differentiation and/or survival of cell types that are not normally derived from retinal progenitors.

(D) A non-transplanted mouse eye showed negative staining for HNA and CRX:tdTomato.
(E) Relative abundance of migratory human cells in different recipient retinal laminae.
(F) Migrating distance of human cell nuclei from the graft edge in different retinal laminae.
(G) Migratory Ku80$^+$ human cells found in the regions flanking the optic nerve (peripapillary migration). White arrows showed representative migratory human cells.
Data were collected from 5 eyes. Statistical data were presented as mean ± SD. Yellow lines in (B), (C), (D), and (G) denote the boundaries of the recipient retina; green lines in (G) denote the optic nerve.

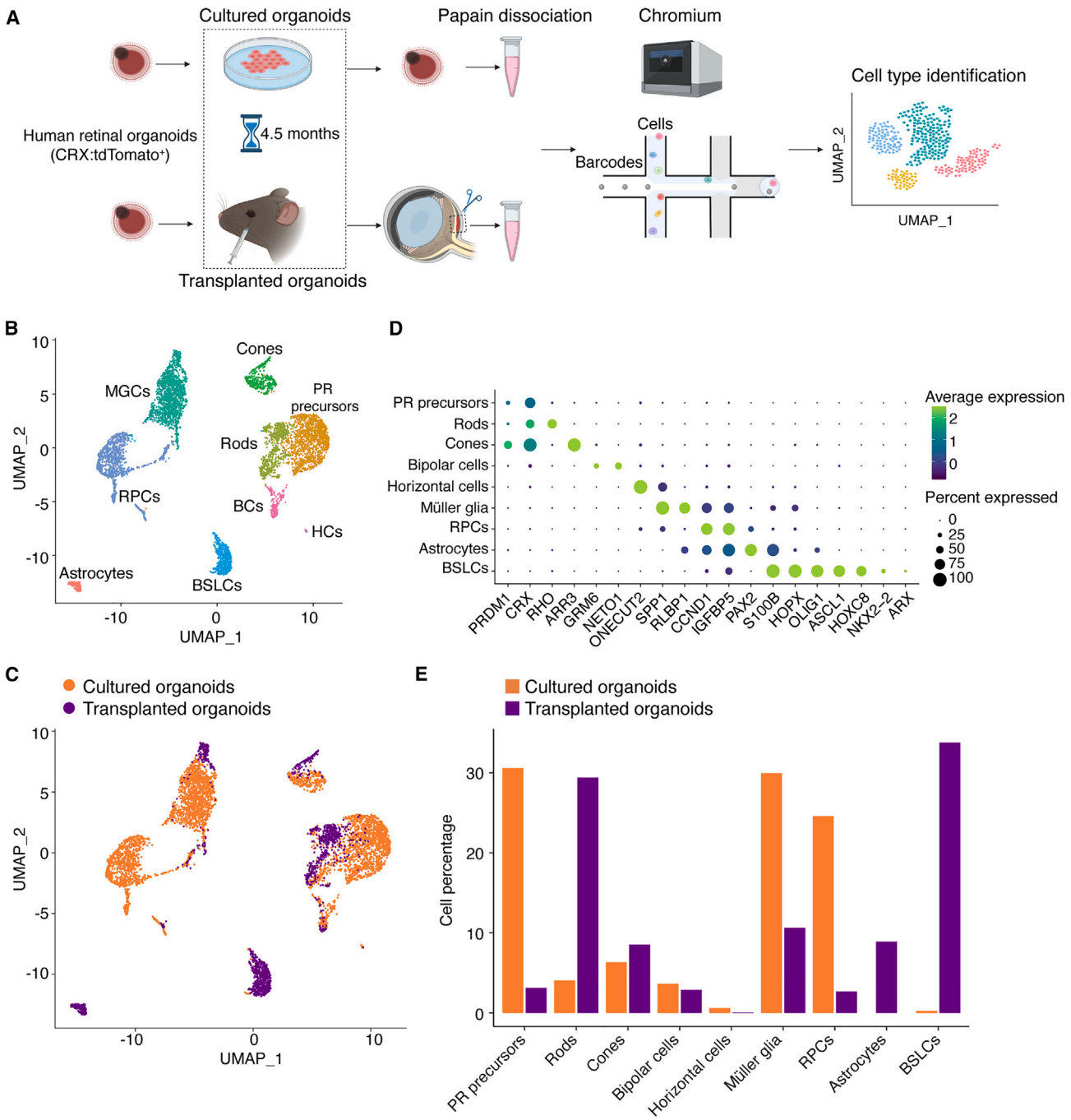

Figure 2. Subretinal microenvironment facilitates the proliferation, differentiation and/or survival of retinal and nonretinal cells

(A) Schematic showing the *in vivo* and *in vitro* conditions of the donor cells analyzed by single-cell RNA sequencing (scRNA-seq).

(B and C) scRNA-seq identified nine transcriptionally distinct cell clusters from the pool of transplanted and cultured retinal organoid cells (n = 5,831 cells).

(D) Dot plots of marker gene expression in the identified cell clusters. Color scale indicates the average gene expression; Dot size represents the percent of positively expressing cells.

(E) The relative abundance of various cell types in transplanted and cultured retinal organoids.

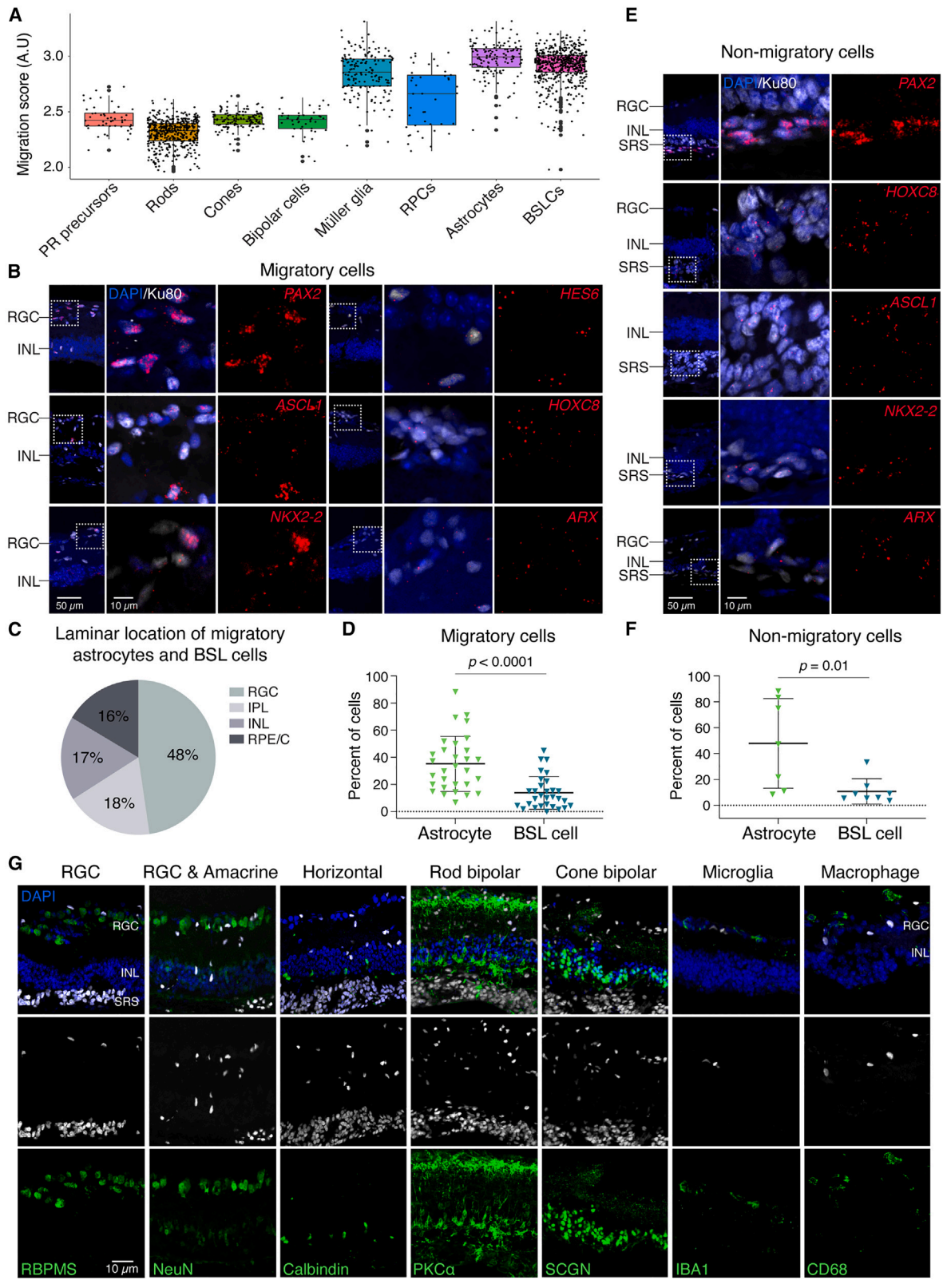

(legend on next page)

Donor-derived migratory cells include astrocytes and brain/spinal cord-like neural precursors

Next, we connected the cell types identified by scRNA-seq analysis to their migratory or non-migratory properties. We computationally aggregated and scored the expression of genes associated with cell motility and migration by Gene Ontology (GO) classification (Data S1). We found that astrocytes and BSL cells had the highest average migration scores (Figure 3A), suggesting that these were the observed migratory cells.

To test this hypothesis, we examined expression of genes including *PAX2* (astrocyte marker), and *HES6*, *ASCL1*, *HOXC8*, *NKX2-2*, and *ARX* (BSL markers), that identify the migratory cells. We observed expression of these genes in migratory cells derived from hESCs (Figures 3B, 3C, and S2). To validate these observations in progeny of a different pluripotent cell lines, we stained for *PAX2*, *HOXC8*, *NKX2-2* in specimens from recipient eyes that were transplanted with human induced pluripotent stem cell (hiPSC)-derived retinal organoid cells. In this context, approximately four months post-transplantation into adult *Rd1/NS* recipient mice, we detected *PAX2*, *HOXC8*, *NKX2-2* in migratory cells (Figure S3). We have not detected the gene expression of human astrocyte (*PAX2*) and BSL (*HES6*, *ASCL1*, *HOXC8*, *NKX2-2*, *ARX*) in non-transplanted *Rd1/NS* control mice (Figure S4). The hESC-derived and hiPSC-derived cells expressing these genes were located in all recipient retinal layers, suggesting that astrocytes and BSL cells derived from both types of pluripotent cells possessed migratory capacity. Among migratory cells, human astrocytes were more abundant than BSL cells (Figure 3D). Among non-migratory cells that remained in the subretinal space within the graft, we also observed astrocytes and BSL cells (Figures 3E and 3F), suggesting that expression of astrocytes or BSL cell-related genes alone was insufficient for migration.

Migratory cells were almost exclusively CRX:tdTomato$^-$, consistent with these cells being astrocytes or BSL cells and not photoreceptor cells (see Figure 1A). Rare CRX:tdTomato$^+$ cells were detected in the RPE/Choroid layer and were possibly misplaced photoreceptors (see Figure 1A). Human migratory cells did not express established markers of RGCs, amacrine cells, horizontal cells, rod and cone bipolar cells, microglia, or macrophages (Figures 3G and S2).

Together, these data suggest that some but not all donor human astrocytes and BSL cells were migratory cells whereas donor photoreceptors and other retinal neurons were non-migratory.

Actively proliferating cells are rare among migratory and non-migratory donor cells

Migratory cells, especially if they are proliferative, may negatively impact the recipient. To determine the influence of the recipient microenvironment on the proliferation of migratory and non-migratory donor cells, we examined expression of the proliferation marker protein Ki-67. As expected, expression of Ki-67 was rarely observed in cultured retinal organoids and was significantly less abundant in transplanted organoids (Figure 4A). The smaller population of proliferating cells in the transplanted organoids suggests that the *in vivo* microenvironment may promote maturation of postmitotic photoreceptor cells.

In eyes with transplanted organoids, 0.7% of non-migratory cells and 1.4% of migratory cells expressed Ki-67 (Figure 4B), and the difference between these values was not statistically significant. We observed that the few Ki-67$^+$ migratory cells occupied all laminae of the recipient retina (Figure 4C).

To identify the proliferating cells, we developed a proliferation scoring system by computationally aggregating the expression level of proliferation-associated genes (Data S2). We found that astrocytes, Müller glia, RPCs, and BSL cells showed the highest proliferation score (Figure 4D), suggesting that these cells were proliferating. To test this hypothesis, we examined expression of Ki-67 in *PAX2*$^+$ (astrocytes), *VSX2*$^+$ (RPCs), and *ASCL1*$^+$ and *HOXC8*$^+$ (BSL) cells. Precise quantification was impractical because of the rarity of double-positive cells. Nevertheless, we found a few migratory *PAX2*$^+$ astrocytes, and very few migratory *ASCL1*$^+$ BSL cells, that were Ki-67$^+$. Proliferating Ki-67$^+$/*VSX2*$^+$ RPCs remained in the subretinal space (Figure 4E).

Taken together, these data suggest that migratory proliferating donor human cells are rare and are mostly astrocytes, and that non-migratory proliferating cells are rare and are mostly RPCs.

Figure 3. Donor-derived migratory cells include astrocytes and brain/spinal cord-like neural precursors

(A) Astrocytes and BSL cells show the highest migration score among the cell types identified in transplanted retinal organoids (n = 3 eyes).
(B) RNAScope showed migratory cells expressing markers of astrocytes (*PAX2*, *HES6*) and BSL cells (*ASCL1*, *HOXC8*, *NKX2-2*, and *ARX*).
(C) Relative abundance of migratory astrocytes and BSL cells in different recipients' retinal laminae.
(D) Quantification of migratory astrocytes and BSL cells in migratory human cells (n = 3 or 4 eyes).
(E and F) RNAScope staining (E) and quantification (F) of non-migratory astrocytes and BSL cells in the subretinal space (SRS) (n = 4 eyes).
(G) Migratory cells negatively expressed markers of RGC (RBPMS, NeuN), amacrine cells (NeuN), horizontal cells (calbindin), rod bipolar cells (PKCα), cone bipolar cells (SCGN), microglia (IBA1), and macrophage (CD68). KU80- and HNA-labeled human cells.
Statistical data were presented as mean ± SD.

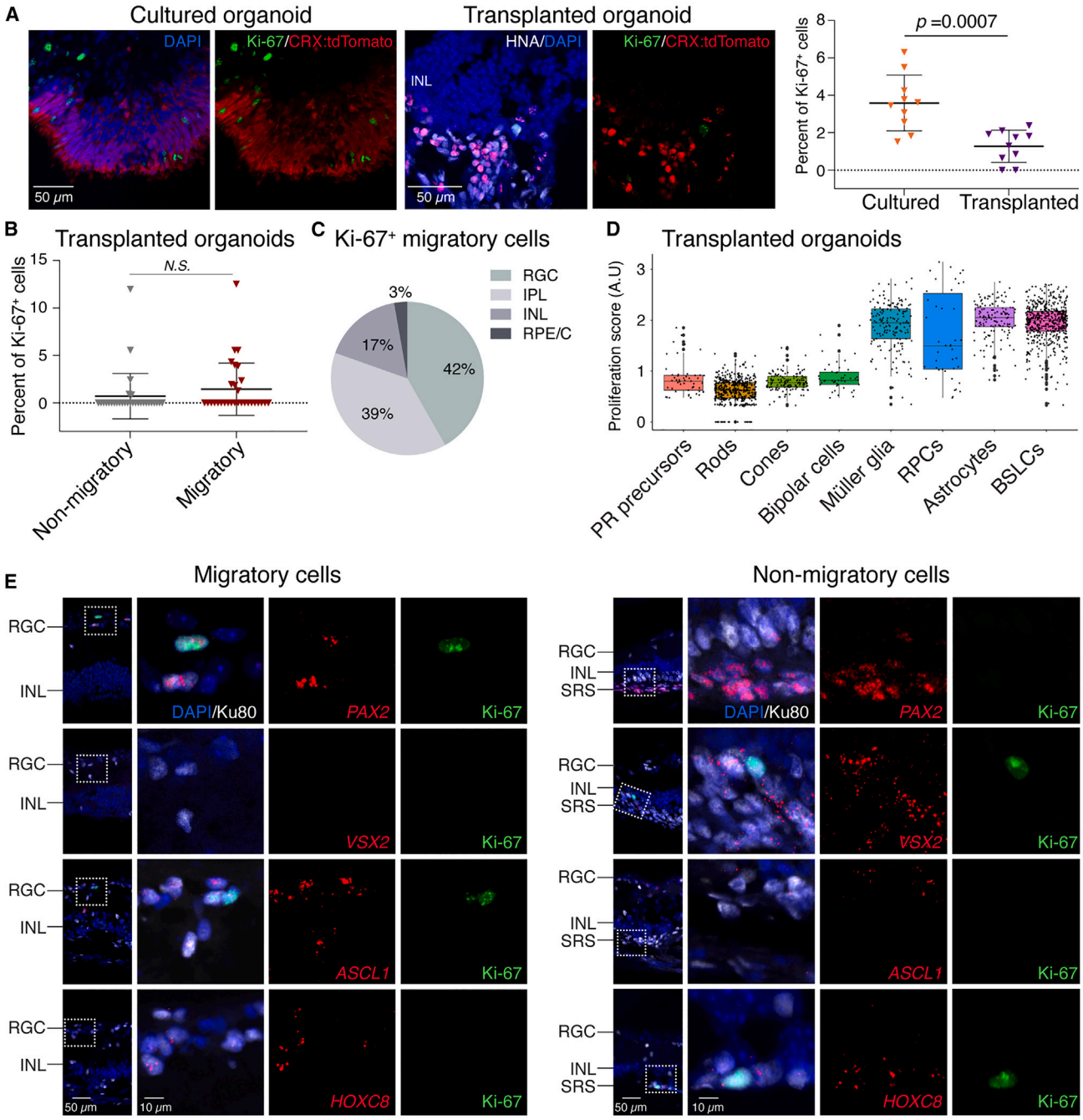

Figure 4. Actively proliferating cells are rare among migratory and non-migratory donor cells

(A) IHC staining showed that Ki-67$^+$ proliferating cells were rare in cultured organoids (n = 4 in one batch) and significantly less in transplanted organoids (n = 3 eyes).

(B) Ki-67$^+$ cells were rare among non-migratory and migratory cells in transplanted retinal organoids (n = 5 eyes).

(C) Relative abundance of migratory Ki-67$^+$ cells in different retinal laminae.

(D) ScRNA-seq analysis showed the highest proliferation score in Müller glia, retinal progenitor cells (RPCs), astrocytes, and BSL cells among the identified cell types in transplanted retinal organoids (n = 3 eyes).

(E) Histological assay showed sparse Ki-67$^+$ cells in migratory astrocytes (*PAX2*$^+$), BSL cells (*ASCL1*$^+$), and non-migratory RPCs (*VSX2*$^+$) and BSL cells (*HOXC8*$^+$) (n = 4 eyes).

Statistical data were presented as mean ± SD.

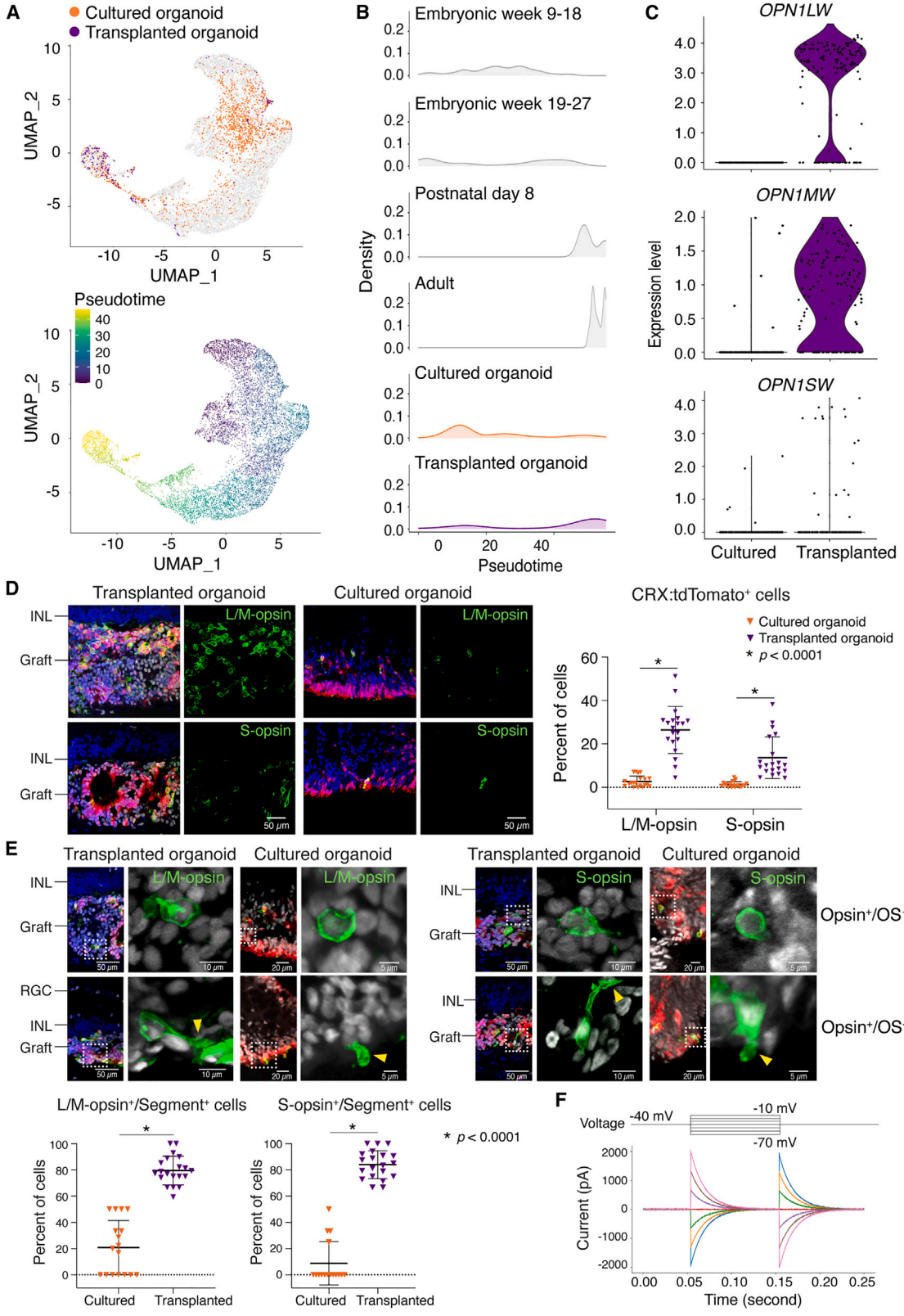

(legend on next page)

In contrast to migrating cells, the subretinal microenvironment induces accelerated maturation of non-migratory rods and cones

Our scRNA-seq analysis suggested that the recipient subretinal space promotes photoreceptor maturation (see Figure 2E). To test this hypothesis, we assessed cone maturation. We evaluated the gene expression profiles of cones from transplanted organoids and cultured organoids using pseudotime analysis, comparing these cells to published datasets of embryonic, postnatal, and adult cones isolated directly from human retina (Lu et al., 2020). The transcriptional profiles suggested that the cones from transplanted organoids resembled adult cones, whereas the cones from cultured organoids more closely resembled embryonic cones (Figures 5A and 5B). Expression of mature cone-specific genes were consistently higher in transplanted than in cultured cones (Figure S5), including all three cone opsins (*OPN1LW*, *OPN1MW*, and *OPN1SW*) (Figure 5C). The proportions of CRX:tdTomato$^+$ cells that expressed L/M-opsin or S-opsin were significantly higher in transplanted organoids (L/M-opsin$^+$, 26.4%; S-opsin$^+$, 13.7%) compared with cultured organoids (L/M-opsin$^+$, 2.7%; S-opsin$^+$, 1.3%) (Figure 5D). Similarly, the fraction of L/M-opsin$^+$ or S-opsin cells$^+$ with inner or outer segments (segment$^+$) was significantly higher in transplanted organoids than cultured organoids (Figure 5E). We measured the intrinsic electrical properties of a transplanted human cone cell and found large capacitance currents (~2 nA), indicating the presence of relatively large cell membrane areas that are normally observed in mature cones (Figure 5F).

Next, we evaluated rod maturation in transplanted organoids and cultured organoids. As with cones, gene expression and pseudotime analysis suggested that rods from transplanted organoids resembled adult rods, whereas rods from cultured organoids resembled embryonic rods (Figures 6A and 6B). Expression of *RHO* (Figure 6C) and other rod-specific genes (Figure S5) was higher in rods from transplanted organoids than cultured organoids. The proportions of CRX:tdTomato$^+$ cells that expressed Rho were significantly higher in transplanted organoids (61.5%) compared with cultured organoids (45.5%) (Figure 6D). Similarly, the fraction of Rho$^+$ cells with inner or outer segments (segment$^+$) was significantly higher in transplanted organoids (87.4%) than cultured organoids (29.8%) (Figure 6E).

Finally, we investigated general features of photoreceptor maturity. Expression of certain synaptic proteins was upregulated in cones and rods in transplanted CRX:tdTomato$^+$ organoids compared with cultured CRX:tdTomato$^+$ organoids (Figure 7A). In CRX:tdTomato$^+$ donor photoreceptors, the number of CtBP2$^+$ puncta, which marks synaptic ribbons, was significantly higher in cells from transplanted organoids compared with cultured retinal organoids (Figure 7B). These data suggest that the recipient subretinal space promotes maturation of rods and cones more effectively than the *in vitro* microenvironment of cultured organoids.

DISCUSSION

In these studies, we observed two major differences between cells from donor retinal organoids transplanted into mice and cells from chronologically equivalent retinal organoids maintained in culture. The transplanted cells were maintained in the degenerative recipient subretinal space for several months, therefore simulating conditions directly relevant for cell-based therapies for photoreceptor dystrophy. The most prominent and unexpected difference was the observation of migratory donor astrocytes and BSL cells in the transplanted cell population. Astrocytes and BSL cells underwent radial migration into, and long-distance tangential migration along, all retinal laminae (apart from the outer nuclear layer of photoreceptor cells that was absent in the degenerate recipients). The migratory astrocytes and BSL cells were generally non-proliferative, although graft-derived retinal progenitors showed proliferation without migration. In contrast to these migratory

Figure 5. The subretinal microenvironment induces accelerated maturation of non-migratory cones

(A) Uniform manifold approximation and projection (UMAP) plots embedded the pseudotime maturation trajectories of cone photoreceptors in transplanted (n = 3 eyes) and cultured retinal organoids (n = 2 form the same batch as the transplanted organoids), comparing to normal human cone development. Cells are colored by cell type (top) and pseudotime (bottom).

(B) Ridge plots showed the transcriptional maturation of transplanted and cultured cone photoreceptors.

(C) Violin plots showed significantly more *OPN1LW*, *OPN1MW*, and *OPN1SW* expression in transplanted than cultured retinal organoids.

(D) Histological analysis of L/M-opsin$^+$ or S-opsin$^+$ photoreceptors in transplanted (n = 4 eyes) and cultured retinal organoids (n = 4 in one batch).

(E) Representative L/M-opsin$^+$ or S-opsin$^+$ cone photoreceptors with (OS$^+$, yellow arrow heads) or without (OS$^-$) outer segments. Quantification showed the fraction of L/M-opsin$^+$ or S-opsin$^+$ cells with inner/outer segment (segment$^+$) in transplanted (n = 4 eyes) and cultured retinal organoids (n = 4 in one batch).

(F) Single-cell patch-clamp recording of a transplanted human cone photoreceptor.

Statistical data were presented as mean ± SD.

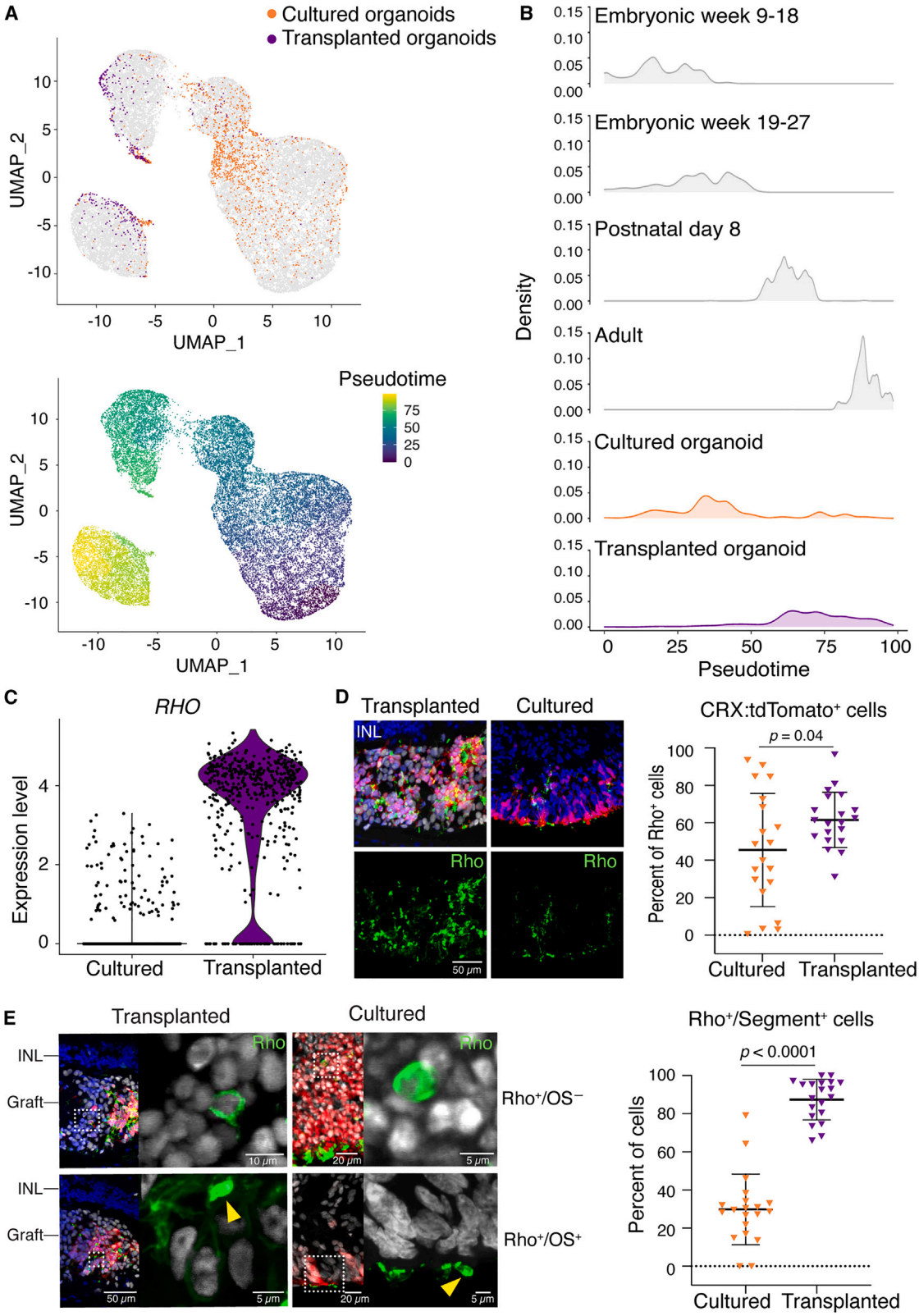

(legend on next page)

cells, transplanted photoreceptors, inner retinal neurons, and Müller glia were non-migratory and remained in the subretinal transplant site. The second major difference between transplanted and cultured organoids pertained to photoreceptor maturity. On the basis of gene expression and morphology, transplanted rods and cones were more mature than photoreceptors from cultured organoids. These data expand our understanding of photoreceptor and non-photoreceptor development in transplanted retinal organoids and highlight the importance of unbiased approaches to cell fate identification and spatial tracking following organoid transplantation.

We considered the possibility that cellular material transfer (Ortin-Martinez et al., 2017; Pearson et al., 2016; Santos-Ferreira et al., 2016; Singh et al., 2014, 2016) of human nucleus-related antigens may have confounded the histological detection of human cells. We believe that the migratory cells in this report are *bona fide* human cells for five reasons. First, all the cells expressing astrocyte and BSCL cell markers were identified by scRNA-seq as being human cells by expression of many different human mRNAs from those of mouse. Second, we used human-specific RNA probes for RNAScope assays used to detect migrating cells. Third, we used two human nuclear-specific antibodies—HNA and Ku80, which target different human nuclear antigens—and found identical features of migration of HNA^+ and $Ku80^+$ cells. Fourth, the uniform and strong intensity of histological staining (HNA and Ku80), essentially iso-intense with the subretinal human cells, also implies that these cells are of human rather than mouse origin. Last, the migratory HNA^+ and $Ku80^+$ cells were generally located at considerable distances from the subretinal donor cell mass, arguing against cellular material transfer which tends to occur among neighboring cells with the potential for direct cell-cell membrane contact.

The migratory astrocytes and BSL cells from transplanted organoids display molecular profiles distinct from cells present in mature cultured organoids. The astrocytes express *PAX2*, which normally delineates optic stalk-derived astrocytes *in vivo* (Wahlin et al., 2021). *PAX2* is also detected in retinal progenitors in early-stage retinal organoids but is undetectable at later stages (Cowan et al., 2020; Lu et al., 2020). Moreover, cultured retinal organoids have not been reported to generate astrocytes *in vitro*. The BSL cells express *ASCL1*, *HOXC8*, *NKX2-2*, and *ARX*. *NKX2-2*- and *ARX*-expressing cells are found in very early-stage retinal organoids, but are not detected after 60 days in culture (Lu et al., 2020). *HOXC8* expression is normally restricted to the posterior spinal cord and is entirely absent from developing human retina and retinal organoids (Cowan et al., 2020; Lu et al., 2020). Though $PAX2^+$ astrocytes and ARX^+ telencephalic interneurons undergo long-distance tangential migration *in vivo* (Paisley and Kay, 2021; Park et al., 2002), astrocyte or BSL identity was not sufficient to induce migration of graft-derived cells, as many astrocytes and BSL cells remained localized in the subretinal space. Our experiments lacked the temporal resolution to determine whether transplantation induced *trans*-differentiation of cells that initially adopted retinal identity or selectively promoted the proliferation and/or survival of small numbers of residual astrocytes and BSL cells that are present at the time of transplantation.

Prior publications have shown migratory transplanted cells, but their capacity to proliferate and migrate long distances were not known. Seiler and colleagues noted migratory human donor cells six months after transplantation of early-stage hESC-derived retinal organoids in the retinal degeneration nude rat (McLelland et al., 2018). Using LMNB2 to identify human donor cells, Lamba and colleagues reported occasional migratory human induced pluripotent stem cell (iPSC)-derived $PAX6^+$ and $GFAP^+$ cells at 2 months post-transplantation (Zhu et al., 2018). In another study, migratory cells were seen just seven days after subretinal delivery of human fetal $CD29^+$/$SSEA1^+$ donor cells (Lakowski et al., 2018), suggesting that migration occurs soon after transplantation. Whether the early-migratory cells are the same as those observed months later is unknown. In the wild-type cat (Singh et al., 2019), enhanced immunosuppression appeared to lead to greater cell migration, suggesting a role of immune cells in restricting this process. It is not known whether migratory donor cells negatively affect recipient retinal

Figure 6. The subretinal microenvironment induces accelerated maturation of non-migratory rods

(A) UMAP plots embedded the pseudotime maturation trajectories of rod photoreceptors in transplanted (n = 3 eyes) and cultured retinal organoids (n = 2 from the same batch as the transplanted organoids), comparing to human rod development. Cells were colored by cell type (top) and pseudotime (bottom).

(B) Ridgeline plot showed the transcriptional maturation of transplanted and cultured rod photoreceptors.

(C) Violin plots showed more *RHO* gene expression in transplanted than cultured retinal organoids.

(D) IHC analysis showed the percent of Rho^+ cells in transplanted (n = 4 eyes) than cultured retinal organoids (n = 4 in one batch).

(E) Representative images showed Rho^+ rod photoreceptors with (OS^+, yellow arrow heads) or without (OS^-) outer segments. Quantification showed the fraction of Rho^+ cells with inner/outer segment ($segment^+$) in transplanted (n = 4 eyes) than cultured retinal organoids (n = 4 in one batch).

Statistical data were presented as mean ± SD.

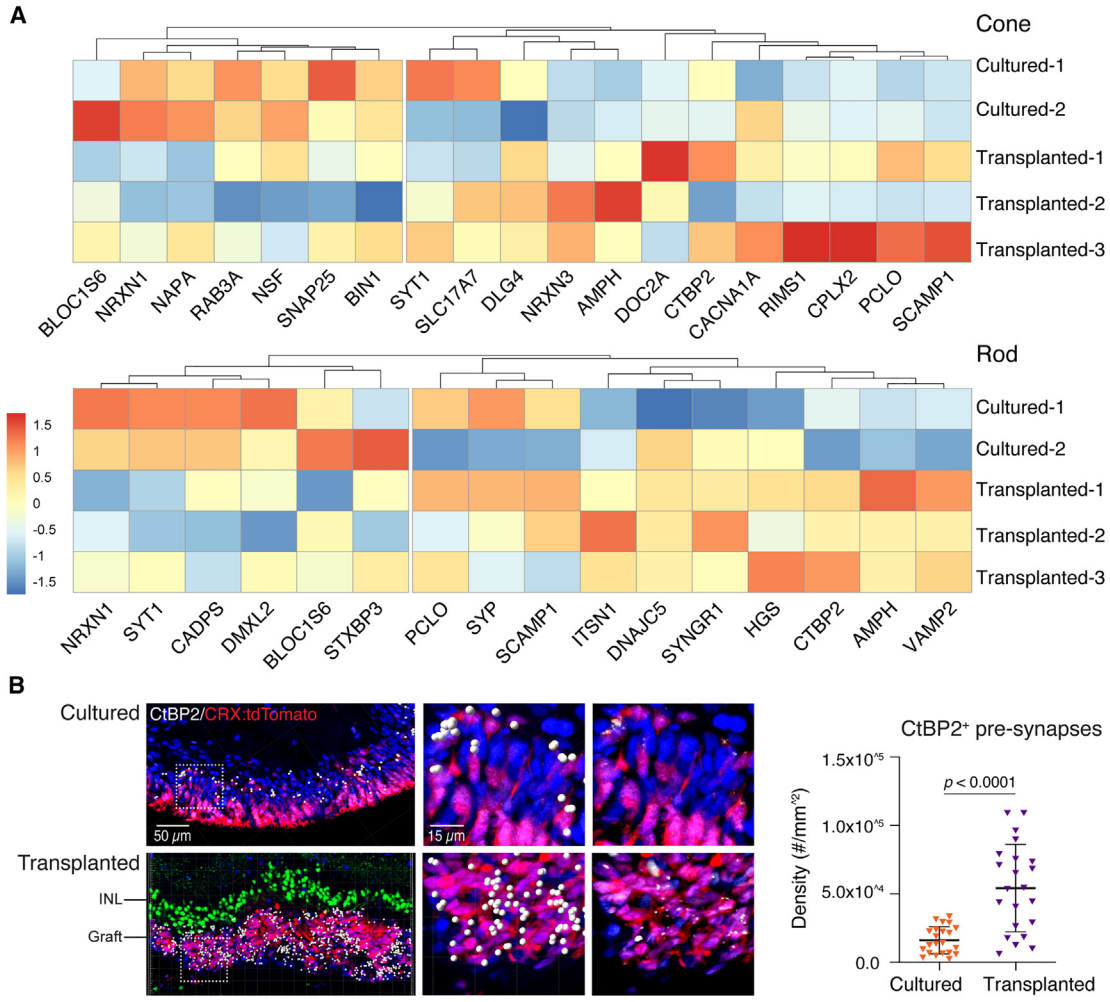

Figure 7. Expression of synaptic proteins is upregulated in transplanted photoreceptors

(A) Heatmaps of synaptic gene expression in transplanted and cultured retinal organoids.

(B) IHC test showed CtBP2$^+$ ribbons synapse in photoreceptors in transplanted (n = 4 eyes) than cultured retinal organoids (n = 4 in one batch). CtBP2$^+$ pre-synapses are highlighted with white dots using Imaris (version 9.1), raw images are on the right panel. IHC staining of SCGN (green) showed the recipient bipolar layer.

Statistical data were presented as mean ± SD.

function or if depletion of astrocyte/BSL precursor cells is required prior to transplantation for maximal therapeutic efficacy.

The cues in the recipient microenvironment that promote cell migration and photoreceptor maturation are not known. Multiple cell-extrinsic cues regulate cell specification in human retinal organoids. Dynamic regulation of thyroid hormone and retinoic acid signaling specifies cone subtypes in human retinal organoids (Eldred et al., 2018; Hadyniak et al., 2021). Though the roles of these cues in the subretinal microenvironment following transplantation is not understood, they potentially regulate photoreceptor specification and maturation.

In conclusion, we found that the murine subretinal microenvironment affects human stem cell-derived retinal organoid cells in two distinct ways. First, the recipient microenvironment facilitates the differentiation and/or survival of cell populations of organoid-derived astrocytes and BSL cells that are capable of radial and tangential migration. Second, the recipient microenvironment promotes the maturation of organoid-derived rod and cone photoreceptors that remain in the subretinal space. These results may inform future research on the consequences of donor cell migration in transplant recipients, methods to purify retinal organoid-derived cells, and pharmacological strategies to accelerate the maturation of donor photoreceptor cells. A deeper understanding of these issues may

help to guide the development of safe and effective clinical treatment involving the replacement or augmentation of human stem cell-derived retinal photoreceptor cells for the purposes of restoring visual function.

EXPERIMENTAL PROCEDURES

Resource availability

Corresponding author

The data that support the findings of this study are available from the corresponding authors Mandeep S. Singh (singhcorrespauth@gmail.com), Seth Blackshaw (sethblackshaw@gmail.com), and Robert J. Johnston (robertjohnston@jhu.edu), upon reasonable request.

Materials availability

This study did not generate new unique materials.

The use of human stem cells was approved by the Johns Hopkins ISCRO (ISCRO00000249) and the University of Colorado Office of Regulatory Compliance. All animal experiments were carried out in accordance with the ARVO Statement for the Use of Animals in Ophthalmic and Vision Research. All procedures were approved by the Johns Hopkins University Animal Care and Use Committee (approval M016M17).

Detailed experimental methods are provided in the supplemental information.

Data and code availability

The raw scRNA-seq data and count matrices generated during this study can be accessed at GEO accession number GSE197847. The merged count matrices and cell metadata are also available for download at https://github.com/csanti88/transplant_human_organoid_retina_2022. Interactive queries of individual gene expression patterns can be performed on the UCSC cell browser at https://xeno-hesc-retina.cells.ucsc.edu (Speir et al., 2021).

SUPPLEMENTAL INFORMATION

Supplemental information can be found online at https://doi.org/10.1016/j.stemcr.2023.04.004.

AUTHOR CONTRIBUTIONS

M.S.S., S.B., and R.J.J. conceived the experiments. Y.V.L., C.P.S., A.S., G.J.K., S.E.H., K.A.H., T.J.C., L.D.O., Z.J., K.V.L., M.F.-B., and S.A.-D. performed the experiments. All the authors contributed to data analysis and approved the final manuscript.

ACKNOWLEDGMENTS

This work was funded by the following funding: National Eye Institute (NEI) R01EY033103 (M.S.S.), Foundation Fighting Blindness (M.S.S.), Stein Innovation Award from Research to Prevent Blindness (S.B.), the Shulsky Foundation (M.S.S.), the Joseph Albert Hekimian Fund (M.S.S.), the Juliette RP Vision Foundation (Y.L.), Gates Frontiers Fund (M.V.C.-S.), The Solich Fund (M.V.C.-S.), *CellSight* Development Fund (M.V.C.S.), Research to Prevent Blindness (unrestricted grant to the Wilmer Eye Institute at Johns Hopkins University, the Clean Energy Institute at Baylor College of Medicine, and the Department of Ophthalmology, University of Colorado), NEI Core Grant EY001765, Visual Sciences Training grant 2T32EY007143 (C.P.S.), National Science Foundation (NSF) DGE-1746891 (K.A.H.), NIH F31EY029157 (S.E.H.), and NEI R01EY030872 (R.J.J.). We thank Dr. David M. Gamm (University of Wisconsin Hospitals) for kindly providing CRX:tdTomato cell line. We thank Dr. Thomas Vincent Johnson III (Johns Hopkins University) for antibody gifts. We thank Dr. Donald J. Zack (Johns Hopkins University) and José Sahel (University of Pittsburgh) for their helpful comments on this paper. We thank Rhonda Griebe and Mary Ellen Pease (Johns Hopkins University) for their kind technical assistance. We thank Wendy Yap for comments on the manuscript. We also thank Brittney Wick, Matthew Speir, and Maximilian Haeussler with their assistance with hosting the data on the UCSC Cell Browser.

CONFLICT OF INTERESTS

M.S.S. is/was a paid advisor to Revision Therapeutics, Johnson & Johnson, Third Rock Ventures, Bayer Healthcare, Novartis Pharmaceuticals, W. L. Gore & Associates, Deerfield, Trinity Partners, Kala Pharmaceuticals, Janssen, and Acucela. M.S.S. has received sponsored research support from Bayer for other research. S.B. receives research support from Genentech, is a co-founder and shareholder in CDI Labs, LLC, and is/was a consultant for Third Rock Ventures and Tenpoint Therapeutics. M.S.S. and R.J.J are co-founders and shareholders in Agnos Therapeutics. These arrangements have been reviewed and approved by the Johns Hopkins University in accordance with its conflict-of-interest policies. M.S.S., S.B., J.Q., R.J.J., Y.V.L., C.P.S., M.V.C.-S., M.F.-B., S.A.-D., and K.V.L. are named as inventors on patents or patent applications assigned to their respective universities.

Received: December 9, 2022
Revised: April 6, 2023
Accepted: April 11, 2023
Published: May 9, 2023

REFERENCES

Aboualizadeh, E., Phillips, M.J., McGregor, J.E., DiLoreto, D.A., Jr., Strazzeri, J.M., Dhakal, K.R., Bateman, B., Jager, L.D., Nilles, K.L., Stuedemann, S.A., et al. (2020). Imaging transplanted photoreceptors in living nonhuman primates with single-cell Resolution. Stem Cell Rep. *15*, 482–497. https://doi.org/10.1016/j.stemcr.2020.06.019.

Assawachananont, J., Mandai, M., Okamoto, S., Yamada, C., Eiraku, M., Yonemura, S., Sasai, Y., and Takahashi, M. (2014). Transplantation of embryonic and induced pluripotent stem cell-derived 3D retinal sheets into retinal degenerative mice. Stem Cell Rep. *2*, 662–674. https://doi.org/10.1016/j.stemcr.2014.03.011.

Bartsch, U., Oriyakhel, W., Kenna, P.F., Linke, S., Richard, G., Petrowitz, B., Humphries, P., Farrar, G.J., and Ader, M. (2008). Retinal cells integrate into the outer nuclear layer and differentiate into mature photoreceptors after subretinal transplantation into adult mice. Exp. Eye Res. *86*, 691–700. https://doi.org/10.1016/j.exer.2008.01.018.

Berger, A.S., Tezel, T.H., Del Priore, L.V., and Kaplan, H.J. (2003). Photoreceptor transplantation in retinitis pigmentosa: short-term follow-up. Ophthalmology *110*, 383–391. https://doi.org/10.1016/S0161-6420(02)01738-4.

Bowes, C., Li, T., Danciger, M., Baxter, L.C., Applebury, M.L., and Farber, D.B. (1990). Retinal degeneration in the rd mouse is caused by a defect in the beta subunit of rod cGMP-phosphodiesterase. Nature *347*, 677–680. https://doi.org/10.1038/347677a0.

Capowski, E.E., Samimi, K., Mayerl, S.J., Phillips, M.J., Pinilla, I., Howden, S.E., Saha, J., Jansen, A.D., Edwards, K.L., Jager, L.D., et al. (2019). Reproducibility and staging of 3D human retinal organoids across multiple pluripotent stem cell lines. Development *146*, dev171686. https://doi.org/10.1242/dev.171686.

Cowan, C.S., Renner, M., De Gennaro, M., Gross-Scherf, B., Goldblum, D., Hou, Y., Munz, M., Rodrigues, T.M., Krol, J., Szikra, T., et al. (2020). Cell types of the human retina and its organoids at single-cell resolution. Cell *182*, 1623–1640.e34. https://doi.org/10.1016/j.cell.2020.08.013.

Das, T., del Cerro, M., Jalali, S., Rao, V.S., Gullapalli, V.K., Little, C., Loreto, D.A., Sharma, S., Sreedharan, A., del Cerro, C., and Rao, G.N. (1999). The transplantation of human fetal neuroretinal cells in advanced retinitis pigmentosa patients: results of a long-term safety study. Exp. Neurol. *157*, 58–68. https://doi.org/10.1006/exnr.1998.6992.

Eiraku, M., Takata, N., Ishibashi, H., Kawada, M., Sakakura, E., Okuda, S., Sekiguchi, K., Adachi, T., and Sasai, Y. (2011). Self-organizing optic-cup morphogenesis in three-dimensional culture. Nature *472*, 51–56. https://doi.org/10.1038/nature09941.

Eldred, K.C., Hadyniak, S.E., Hussey, K.A., Brenerman, B., Zhang, P.W., Chamling, X., Sluch, V.M., Welsbie, D.S., Hattar, S., Taylor, J., et al. (2018). Thyroid hormone signaling specifies cone subtypes in human retinal organoids. Science *362*, eaau6348. https://doi.org/10.1126/science.aau6348.

Foik, A.T., Lean, G.A., Scholl, L.R., McLelland, B.T., Mathur, A., Aramant, R.B., Seiler, M.J., and Lyon, D.C. (2018). Detailed visual cortical responses generated by retinal sheet transplants in rats with severe retinal degeneration. J. Neurosci. *38*, 10709–10724. https://doi.org/10.1523/JNEUROSCI.1279-18.2018.

Gasparini, S.J., Tessmer, K., Reh, M., Wieneke, S., Carido, M., Völkner, M., Borsch, O., Swiersy, A., Zuzic, M., Goureau, O., et al. (2022). Transplanted human cones incorporate into the retina and function in a murine cone degeneration model. J. Clin. Invest. *132*, e154619. https://doi.org/10.1172/JCI154619.

Ghosh, F., Wong, F., Johansson, K., Bruun, A., and Petters, R.M. (2004). Transplantation of full-thickness retina in the rhodopsin transgenic pig. Retina *24*, 98–109.

Gonzalez-Cordero, A., West, E.L., Pearson, R.A., Duran, Y., Carvalho, L.S., Chu, C.J., Naeem, A., Blackford, S.J.I., Georgiadis, A., Lakowski, J., et al. (2013). Photoreceptor precursors derived from three-dimensional embryonic stem cell cultures integrate and mature within adult degenerate retina. Nat. Biotechnol. *31*, 741–747. https://doi.org/10.1038/nbt.2643.

Gouras, P., Du, J., Kjeldbye, H., Yamamoto, S., and Zack, D.J. (1994). Long-term photoreceptor transplants in dystrophic and normal mouse retina. Invest. Ophthalmol. Vis. Sci. *35*, 3145–3153.

Hadyniak, S.E., Eldred, K.C., Brenerman, B., Hussey, K.A., McCoy, R.C., Sauria, M.E.G., Kuchenbecker, J.A., Neitz, M., Neitz, J., Taylor, J., and Johnston, R.J. (2021). Temporal regulation of green and red cone specification in human retinas and retinal organoids. Preprint at bioRxiv. https://doi.org/10.1101/2021.03.30.437763.

Hambright, D., Park, K.Y., Brooks, M., McKay, R., Swaroop, A., and Nasonkin, I.O. (2012). Long-term survival and differentiation of retinal neurons derived from human embryonic stem cell lines in un-immunosuppressed mouse retina. Mol. Vis. *18*, 920–936.

Humayun, M.S., de Juan, E., Jr., del Cerro, M., Dagnelie, G., Radner, W., Sadda, S.R., and del Cerro, C. (2000). Human neural retinal transplantation. Invest Ophthalmol Vis Sci *41*, 3100–3106.

jCyte, I., and California Institute for Regenerative, M. (2020). Safety and efficacy of intravitreal injection of human retinal progenitor cells in adults with retinitis pigmentosa. https://ClinicalTrials.gov/show/NCT03073733.

Kaewkhaw, R., Kaya, K.D., Brooks, M., Homma, K., Zou, J., Chaitankar, V., Rao, M., and Swaroop, A. (2015). Transcriptome dynamics of developing photoreceptors in three-dimensional retina cultures recapitulates temporal sequence of human cone and rod differentiation revealing cell surface markers and gene networks. Stem Cell. *33*, 3504–3518. https://doi.org/10.1002/stem.2122.

Kalargyrou, A.A., Basche, M., Hare, A., West, E.L., Smith, A.J., Ali, R.R., and Pearson, R.A. (2021). Nanotube-like processes facilitate material transfer between photoreceptors. EMBO Rep. *22*, e53732. https://doi.org/10.15252/embr.202153732.

Klassen, H., Kiilgaard, J.F., Zahir, T., Ziaeian, B., Kirov, I., Scherfig, E., Warfvinge, K., and Young, M.J. (2007). Progenitor cells from the porcine neural retina express photoreceptor markers after transplantation to the subretinal space of allorecipients. Stem Cell. *25*, 1222–1230. https://doi.org/10.1634/stemcells.2006-0541.

Klassen, H.J., Ng, T.F., Kurimoto, Y., Kirov, I., Shatos, M., Coffey, P., and Young, M.J. (2004). Multipotent retinal progenitors express developmental markers, differentiate into retinal neurons, and preserve light-mediated behavior. Invest. Ophthalmol. Vis. Sci. *45*, 4167–4173. https://doi.org/10.1167/iovs.04-0511.

Kwan, A.S., Wang, S., and Lund, R.D. (1999). Photoreceptor layer reconstruction in a rodent model of retinal degeneration. Exp. Neurol. *159*, 21–33. https://doi.org/10.1006/exnr.1999.7157.

Lakowski, J., Welby, E., Budinger, D., Di Marco, F., Di Foggia, V., Bainbridge, J.W.B., Wallace, K., Gamm, D.M., Ali, R.R., and Sowden, J.C. (2018). Isolation of human photoreceptor precursors via a cell surface marker panel from stem cell-derived retinal organoids and fetal retinae. Stem Cell. *36*, 709–722. https://doi.org/10.1002/stem.2775.

Lamba, D.A., Gust, J., and Reh, T.A. (2009). Transplantation of human embryonic stem cell-derived photoreceptors restores some visual function in Crx-deficient mice. Cell Stem Cell *4*, 73–79. https://doi.org/10.1016/j.stem.2008.10.015.

Lin, B., McLelland, B.T., Mathur, A., Aramant, R.B., and Seiler, M.J. (2018). Sheets of human retinal progenitor transplants improve vision in rats with severe retinal degeneration. Exp. Eye Res. *174*, 13–28. https://doi.org/10.1016/j.exer.2018.05.017.

Liu, S., Qu, Y., Stewart, T.J., Howard, M.J., Chakrabortty, S., Holekamp, T.F., and McDonald, J.W. (2000). Embryonic stem cells

differentiate into oligodendrocytes and myelinate in culture and after spinal cord transplantation. Proc. Natl. Acad. Sci. USA *97*, 6126–6131. https://doi.org/10.1073/pnas.97.11.6126.

Liu, Y., Chen, S.J., Li, S.Y., Qu, L.H., Meng, X.H., Wang, Y., Xu, H.W., Liang, Z.Q., and Yin, Z.Q. (2017). Long-term safety of human retinal progenitor cell transplantation in retinitis pigmentosa patients. Stem Cell Res. Ther. *8*, 209. https://doi.org/10.1186/s13287-017-0661-8.

Lu, Y., Shiau, F., Yi, W., Lu, S., Wu, Q., Pearson, J.D., Kallman, A., Zhong, S., Hoang, T., Zuo, Z., et al. (2020). Single-cell analysis of human retina identifies evolutionarily conserved and species-specific mechanisms controlling development. Dev. Cell *53*, 473–491.e9. https://doi.org/10.1016/j.devcel.2020.04.009.

Luo, J., Baranov, P., Patel, S., Ouyang, H., Quach, J., Wu, F., Qiu, A., Luo, H., Hicks, C., Zeng, J., et al. (2014). Human retinal progenitor cell transplantation preserves vision. J. Biol. Chem. *289*, 6362–6371. https://doi.org/10.1074/jbc.M113.513713.

MacLaren, R.E., Pearson, R.A., MacNeil, A., Douglas, R.H., Salt, T.E., Akimoto, M., Swaroop, A., Sowden, J.C., and Ali, R.R. (2006). Retinal repair by transplantation of photoreceptor precursors. Nature *444*, 203–207. https://doi.org/10.1038/nature05161.

Mandai, M., Fujii, M., Hashiguchi, T., Sunagawa, G.A., Ito, S.I., Sun, J., Kaneko, J., Sho, J., Yamada, C., and Takahashi, M. (2017). iPSC-derived retina transplants improve vision in rd1 end-stage retinal-degeneration mice (vol 8, pg 69, 2017). Stem Cell Rep. *8*, 1112–1113. https://doi.org/10.1016/j.stemcr.2017.03.024.

McLelland, B.T., Lin, B., Mathur, A., Aramant, R.B., Thomas, B.B., Nistor, G., Keirstead, H.S., and Seiler, M.J. (2018). Transplanted hESC-derived retina organoid sheets differentiate, integrate, and improve visual function in retinal degenerate rats. Invest. Ophthalmol. Vis. Sci. *59*, 2586–2603. https://doi.org/10.1167/iovs.17-23646.

Nakano, T., Ando, S., Takata, N., Kawada, M., Muguruma, K., Sekiguchi, K., Saito, K., Yonemura, S., Eiraku, M., and Sasai, Y. (2012). Self-formation of optic cups and storable stratified neural retina from human ESCs. Cell Stem Cell *10*, 771–785. https://doi.org/10.1016/j.stem.2012.05.009.

Ortin-Martinez, A., Tsai, E.L.S., Nickerson, P.E., Bergeret, M., Lu, Y., Smiley, S., Comanita, L., and Wallace, V.A. (2017). A reinterpretation of cell transplantation: GFP transfer from donor to host photoreceptors. Stem Cell. *35*, 932–939. https://doi.org/10.1002/stem.2552.

Ortin-Martinez, A., Yan, N.E., Tsai, E.L.S., Comanita, L., Gurdita, A., Tachibana, N., Liu, Z.C., Lu, S., Dolati, P., Pokrajac, N.T., et al. (2021). Photoreceptor nanotubes mediate the in vivo exchange of intracellular material. EMBO J. *40*, e107264. https://doi.org/10.15252/embj.2020107264.

Paisley, C.E., and Kay, J.N. (2021). Seeing stars: development and function of retinal astrocytes. Dev. Biol. *478*, 144–154. https://doi.org/10.1016/j.ydbio.2021.07.007.

Park, H.T., Wu, J., and Rao, Y. (2002). Molecular control of neuronal migration. Bioessays *24*, 821–827. https://doi.org/10.1002/bies.10141.

Pearson, R.A., Barber, A.C., Rizzi, M., Hippert, C., Xue, T., West, E.L., Duran, Y., Smith, A.J., Chuang, J.Z., Azam, S.A., et al. (2012). Restoration of vision after transplantation of photoreceptors. Nature *485*, 99–103. https://doi.org/10.1038/nature10997.

Pearson, R.A., Gonzalez-Cordero, A., West, E.L., Ribeiro, J.R., Aghaizu, N., Goh, D., Sampson, R.D., Georgiadis, A., Waldron, P.V., Duran, Y., et al. (2016). Donor and host photoreceptors engage in material transfer following transplantation of post-mitotic photoreceptor precursors. Nat. Commun. *7*, 13029. https://doi.org/10.1038/ncomms13029.

Phillips, M.J., Jiang, P., Howden, S., Barney, P., Min, J., York, N.W., Chu, L.F., Capowski, E.E., Cash, A., Jain, S., et al. (2018). A novel approach to single cell RNA-sequence analysis facilitates in silico gene reporting of human pluripotent stem cell-derived retinal cell types. Stem Cell. *36*, 313–324. https://doi.org/10.1002/stem.2755.

Poggi, L., Vitorino, M., Masai, I., and Harris, W.A. (2005). Influences on neural lineage and mode of division in the zebrafish retina in vivo. J. Cell Biol. *171*, 991–999. https://doi.org/10.1083/jcb.200509098.

ReNeuron, L. (2022). Safety and tolerability of hRPC in retinitis pigmentosa. https://ClinicalTrials.gov/show/NCT02464436.

Santos-Ferreira, T., Llonch, S., Borsch, O., Postel, K., Haas, J., and Ader, M. (2016). Retinal transplantation of photoreceptors results in donor-host cytoplasmic exchange. Nat. Commun. *7*, 13028. https://doi.org/10.1038/ncomms13028.

Scheffler, B., Schmandt, T., Schröder, W., Steinfarz, B., Husseini, L., Wellmer, J., Seifert, G., Karram, K., Beck, H., Blümcke, I., et al. (2003). Functional network integration of embryonic stem cell-derived astrocytes in hippocampal slice cultures. Development *130*, 5533–5541. https://doi.org/10.1242/dev.00714.

Seiler, M.J., Aramant, R.B., Jones, M.K., Ferguson, D.L., Bryda, E.C., and Keirstead, H.S. (2014). A new immunodeficient pigmented retinal degenerate rat strain to study transplantation of human cells without immunosuppression. Graefes Arch. Clin. Exp. Ophthalmol. *252*, 1079–1092. https://doi.org/10.1007/s00417-014-2638-y.

Seiler, M.J., Lin, R.E., McLelland, B.T., Mathur, A., Lin, B., Sigman, J., De Guzman, A.T., Kitzes, L.M., Aramant, R.B., and Thomas, B.B. (2017). Vision recovery and connectivity by fetal retinal sheet transplantation in an immunodeficient retinal degenerate rat model. Invest. Ophthalmol. Vis. Sci. *58*, 614–630. https://doi.org/10.1167/iovs.15-19028.

Shirai, H., Mandai, M., Matsushita, K., Kuwahara, A., Yonemura, S., Nakano, T., Assawachananont, J., Kimura, T., Saito, K., Terasaki, H., et al. (2016). Transplantation of human embryonic stem cell-derived retinal tissue in two primate models of retinal degeneration. Proc. Natl. Acad. Sci. USA *113*, E81–E90. https://doi.org/10.1073/pnas.1512590113.

Singh, M.S., Aslam, S.A., Duncan, I.L., Cramer, A.O., Barnard, A.R., and MacLaren, R.E. (2014). Cell fusion following photoreceptor transplantation into the non-degenerate retina. Invest. Ophth. Vis. Sci. *55*, 3989.

Singh, M.S., Balmer, J., Barnard, A.R., Aslam, S.A., Moralli, D., Green, C.M., Barnea-Cramer, A., Duncan, I., and MacLaren, R.E. (2016). Transplanted photoreceptor precursors transfer proteins

to host photoreceptors by a mechanism of cytoplasmic fusion. Nat. Commun. *7*, 13537. https://doi.org/10.1038/ncomms13537.

Singh, M.S., Charbel Issa, P., Butler, R., Martin, C., Lipinski, D.M., Sekaran, S., Barnard, A.R., and MacLaren, R.E. (2013). Reversal of end-stage retinal degeneration and restoration of visual function by photoreceptor transplantation. Proc. Natl. Acad. Sci. USA *110*, 1101–1106. https://doi.org/10.1073/pnas.1119416110.

Singh, R.K., Occelli, L.M., Binette, F., Petersen-Jones, S.M., and Nasonkin, I.O. (2019). Transplantation of human embryonic stem cell-derived retinal tissue in the subretinal space of the cat eye. Stem Cells Dev. *28*, 1151–1166. https://doi.org/10.1089/scd.2019.0090.

Soucy, J., Oswald, J., and Baranov, P.Y. (2021). SDF1 directs donor retinal ganglion cell migration into the retina following allotransplantation in mice. Invest. Ophthalmol. Vis. Sci. *62*, 2782.

Speir, M.L., Bhaduri, A., Markov, N.S., Moreno, P., Nowakowski, T.J., Papatheodorou, I., Pollen, A.A., Raney, B.J., Seninge, L., Kent, W.J., and Haeussler, M. (2021). UCSC cell browser: visualize your single-cell data. Bioinformatics *37*, 4578–4580. https://doi.org/10.1093/bioinformatics/btab503.

Srivastava, A.S., Shenouda, S., Mishra, R., and Carrier, E. (2006). Transplanted embryonic stem cells successfully survive, proliferate, and migrate to damaged regions of the mouse brain. Stem Cell. *24*, 1689–1694. https://doi.org/10.1634/stemcells.2005-0531.

Tabar, V., Panagiotakos, G., Greenberg, E.D., Chan, B.K., Sadelain, M., Gutin, P.H., and Studer, L. (2005). Migration and differentiation of neural precursors derived from human embryonic stem cells in the rat brain. Nat. Biotechnol. *23*, 601–606. https://doi.org/10.1038/nbt1088.

Thomas, B.B., Lin, B., Martinez-Camarillo, J.C., Zhu, D., McLelland, B.T., Nistor, G., Keirstead, H.S., Humayun, M.S., and Seiler, M.J. (2021). Co-grafts of human embryonic stem cell derived retina organoids and retinal pigment epithelium for retinal reconstruction in immunodeficient retinal degenerate royal college of surgeons rats. Front. Neurosci. *15*, 752958. https://doi.org/10.3389/fnins.2021.752958.

Tu, H.-Y., Watanabe, T., Shirai, H., Yamasaki, S., Kinoshita, M., Matsushita, K., Hashiguchi, T., Onoe, H., Matsuyama, T., Kuwahara, A., et al. (2019). Medium- to long-term survival and functional examination of human iPSC-derived retinas in rat and primate models of retinal degeneration. EBioMedicine *39*, 562–574. https://doi.org/10.1016/j.ebiom.2018.11.028.

Tucker, B.A., Mullins, R.F., Streb, L.M., Anfinson, K., Eyestone, M.E., Kaalberg, E., Riker, M.J., Drack, A.V., Braun, T.A., and Stone, E.M. (2013). Patient-specific iPSC-derived photoreceptor precursor cells as a means to investigate retinitis pigmentosa. Elife *2*, e00824. https://doi.org/10.7554/eLife.00824.

Turner, D.L., and Cepko, C.L. (1987). A common progenitor for neurons and glia persists in rat retina late in development. Nature *328*, 131–136. https://doi.org/10.1038/328131a0.

Turner, D.L., Snyder, E.Y., and Cepko, C.L. (1990). Lineage-independent determination of cell type in the embryonic mouse retina. Neuron *4*, 833–845. https://doi.org/10.1016/0896-6273(90)90136-4.

Wahlin, K.J., Cheng, J., Jurlina, S.L., Jones, M.K., Dash, N.R., Ogata, A., Kibria, N., Ray, S., Eldred, K.C., Kim, C., et al. (2021). CRISPR generated SIX6 and POU4F2 reporters allow identification of brain and optic transcriptional differences in human PSC-derived organoids. Front. Cell Dev. Biol. *9*, 764725. https://doi.org/10.3389/fcell.2021.764725.

Wahlin, K.J., Maruotti, J.A., Sripathi, S.R., Ball, J., Angueyra, J.M., Kim, C., Grebe, R., Li, W., Jones, B.W., and Zack, D.J. (2017). Photoreceptor outer segment-like structures in long-term 3D retinas from human pluripotent stem cells. Sci. Rep. *7*, 766. https://doi.org/10.1038/s41598-017-00774-9.

Yamasaki, S., Tu, H.Y., Matsuyama, T., Horiuchi, M., Hashiguchi, T., Sho, J., Kuwahara, A., Kishino, A., Kimura, T., Takahashi, M., and Mandai, M. (2022). A Genetic modification that reduces ON-bipolar cells in hESC-derived retinas enhances functional integration after transplantation. iScience *25*, 103657. https://doi.org/10.1016/j.isci.2021.103657.

Yang, P., Seiler, M.J., Aramant, R.B., and Whittemore, S.R. (2002). Differential lineage restriction of rat retinal progenitor cells in vitro and in vivo. J. Neurosci. Res. *69*, 466–476. https://doi.org/10.1002/jnr.10320.

Yang, Y., Mohand-Said, S., Léveillard, T., Fontaine, V., Simonutti, M., and Sahel, J.A. (2010). Transplantation of photoreceptor and total neural retina preserves cone function in P23H rhodopsin transgenic rat. PLoS One *5*, e13469. https://doi.org/10.1371/journal.pone.0013469.

Zhong, X., Gutierrez, C., Xue, T., Hampton, C., Vergara, M.N., Cao, L.H., Peters, A., Park, T.S., Zambidis, E.T., Meyer, J.S., et al. (2014). Generation of three-dimensional retinal tissue with functional photoreceptors from human iPSCs. Nat. Commun. *5*, 4047. https://doi.org/10.1038/ncomms5047.

Zhou, L., Wang, W., Liu, Y., Fernandez de Castro, J., Ezashi, T., Telugu, B.P.V.L., Roberts, R.M., Kaplan, H.J., and Dean, D.C. (2011). Differentiation of induced pluripotent stem cells of swine into rod photoreceptors and their integration into the retina. Stem Cell. *29*, 972–980. https://doi.org/10.1002/stem.637.

Zhou, P.-Y., Peng, G.-H., Xu, H., and Yin, Z.Q. (2015). c-Kit$^+$ cells isolated from human fetal retinas represent a new population of retinal progenitor cells. J. Cell Sci. *128*, 2169–2178. https://doi.org/10.1242/jcs.169086.

Zhu, J., Reynolds, J., Garcia, T., Cifuentes, H., Chew, S., Zeng, X., and Lamba, D.A. (2018). Generation of transplantable retinal photoreceptors from a current good manufacturing practice-manufactured human induced pluripotent stem cell line. Stem Cells Transl. Med. *7*, 210–219. https://doi.org/10.1002/sctm.17-0205.

Zou, T., Gao, L., Zeng, Y., Li, Q., Li, Y., Chen, S., Hu, X., Chen, X., Fu, C., Xu, H., and Yin, Z.Q. (2019). Organoid-derived C-Kit/SSEA4 human retinal progenitor cells promote a protective retinal microenvironment during transplantation in rodents. Nat. Commun. *10*, 1205. https://doi.org/10.1038/s41467-019-08961-0.

Stem Cell Reports, Volume *18*

Supplemental Information

Single-cell transcriptome analysis of xenotransplanted human retinal organoids defines two migratory cell populations of nonretinal origin

Ying V. Liu, Clayton P. Santiago, Akin Sogunro, Gregory J. Konar, Ming-wen Hu, Minda M. McNally, Yu-chen Lu, Miguel Flores-Bellver, Silvia Aparicio-Domingo, Kang V. Li, Zhuo-lin Li, Dzhalal Agakishiev, Sarah E. Hadyniak, Katarzyna A. Hussey, Tyler J. Creamer, Linda D. Orzolek, Derek Teng, M. Valeria Canto-Soler, Jiang Qian, Zheng Jiang, Robert J. Johnston Jr., Seth Blackshaw, and Mandeep S. Singh

Supplementary Materials

Single-cell transcriptome analysis of xenotransplanted human retinal organoids defines two migratory cell populations of nonretinal origin

Ying V. Liu, *et al*.

Supplemental Figure 1

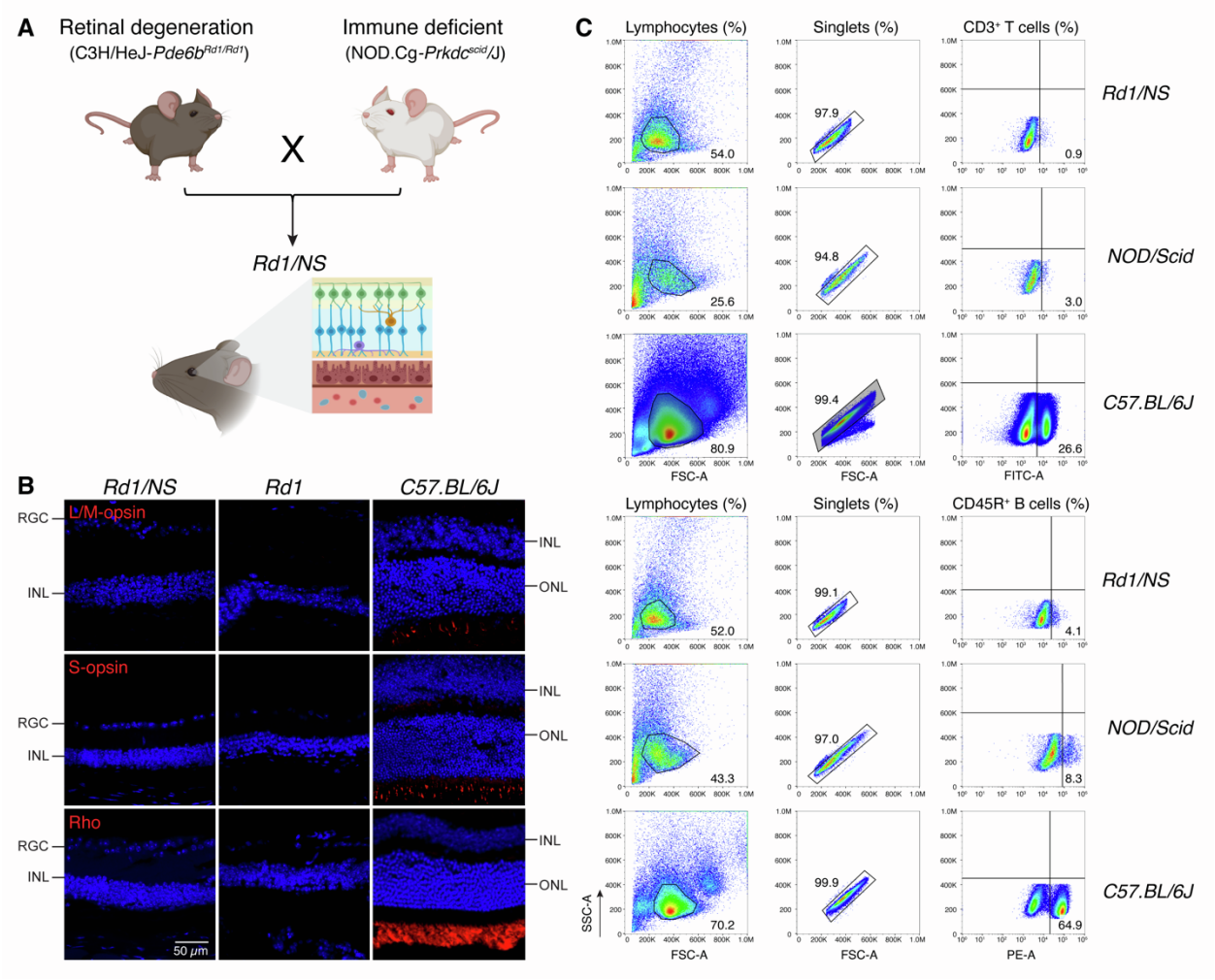

Fig. S1. Breeding and phenotyping of the recipient *Rd1/NS* mice. (A) Schematic showed the recipient *Rd1/NS* mice were generated by crossbreeding C3H/HeJ-*Pde6b*$^{Rd/Rd11}$ (*Rd1)* and NOD.Cg-*Prkdc*^{scid}/J (*NOD/Scid*) mice. **(B)** IHC staining showed fully degenerated photoreceptor cells and negative expression of L/M-opsin, S-opsin, and Rhodopsin (Rho) in adult *Rd1/NS* mice

and *Rd1* mice. *C57.BL/6J* mice served as *wild-type* controls. **(C)** Flow cytometry analysis showed the deficiency of $CD3^+$ T cells and $CD45R^+$ B cells in *Rd1/NS* mice, corresponding to the immune deficient phenotype of *NOD/Scid* mice. *C57.BL/6J* mice served as *wild-type* controls. N= 4 eyes per group.

Supplemental Figure 2

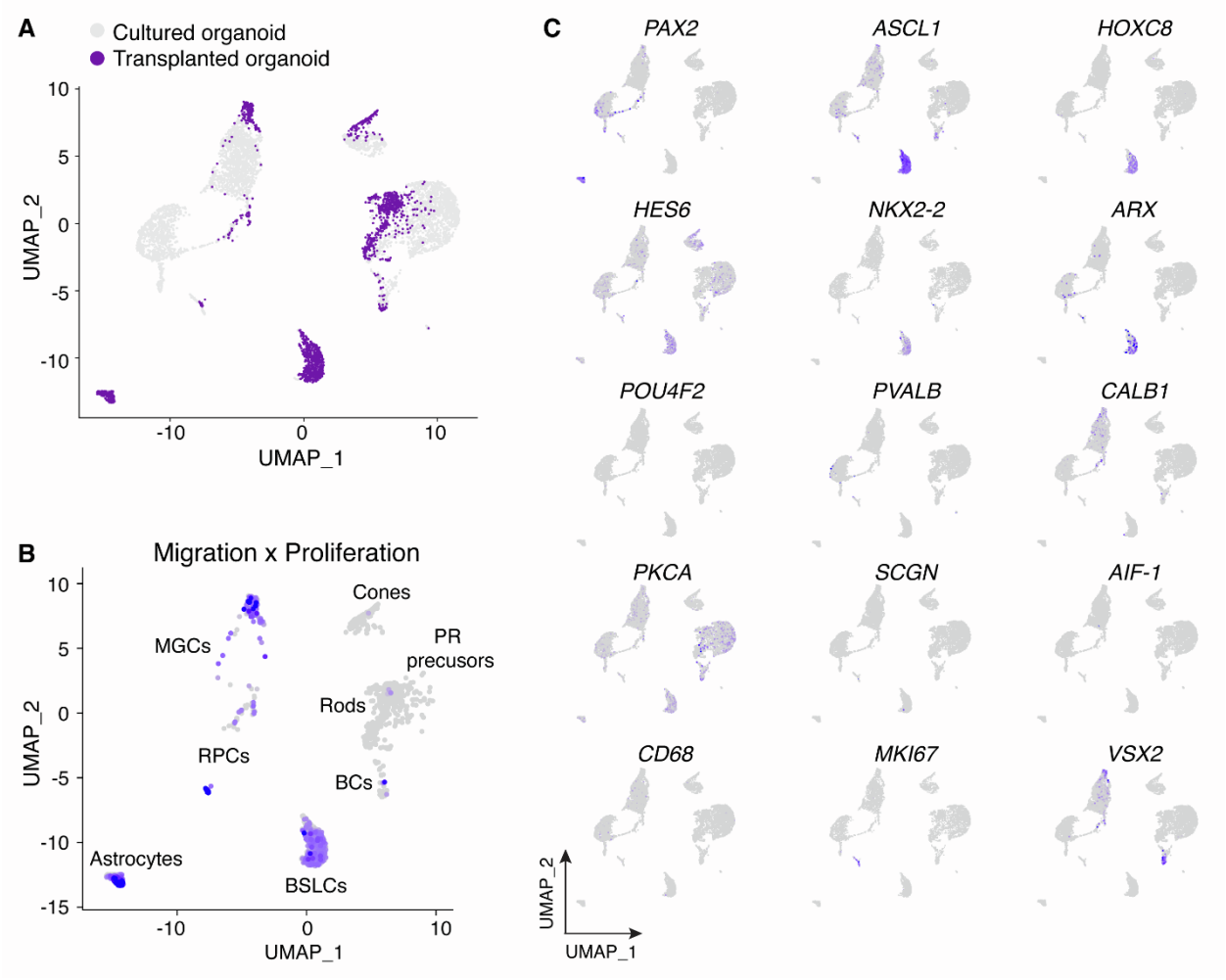

Fig. S2. UMAP plots of migration and proliferation cell clusters. (A) UMAP plot colored cell clusters of cultured (grey, n=2 organoids from one batch) and transplanted retinal organoids (purple, n=3 transplanted eyes). **(B)** UMAP plot colored cell clusters sharing transcriptomic characteristics of migration and proliferation. **(C)** UMAP plots displayed the expression of marker genes in cell clusters of transplanted and cultured retinal organoids.

Supplemental Figure 3

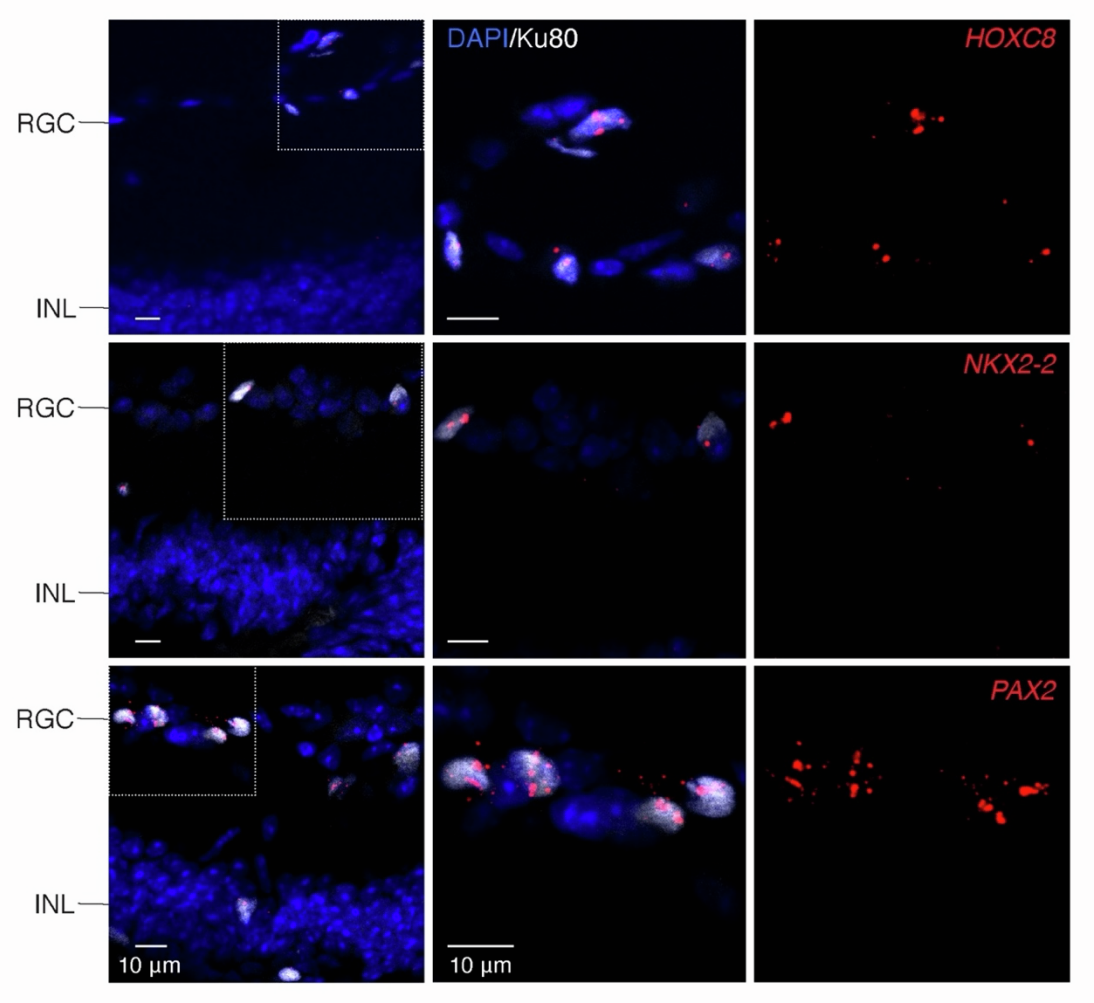

Fig. S3. Human iPSC donor-derived migratory cells include astrocytes and brain/spinal cord-like neural precursors. Migratory cells from human iPSC-derived retinal organoid grafts (n=3 organoids from one iPSC batch, distinct from the H9 ESC-derived organoids used in Fig. 1-7, Fig. S1-S2, and Fig. S5-S6) were detected in the RGC layer and INL of recipient mouse retinae by human nuclear specific antibody Ku80 staining. RNAscope staining showed migratory cells expressing markers of BSL cells *(HOXC8, NKX2-2*) and astrocytes (*PAX2*), consistent with the characteristics of those migratory cells in Crx:tdTomato^{+} hESC-derived retinal organoid grafts. *Abbreviation: RGC: retinal gaglion cell layer; INL: inner nuclear layer.*

Supplemental Figure 4

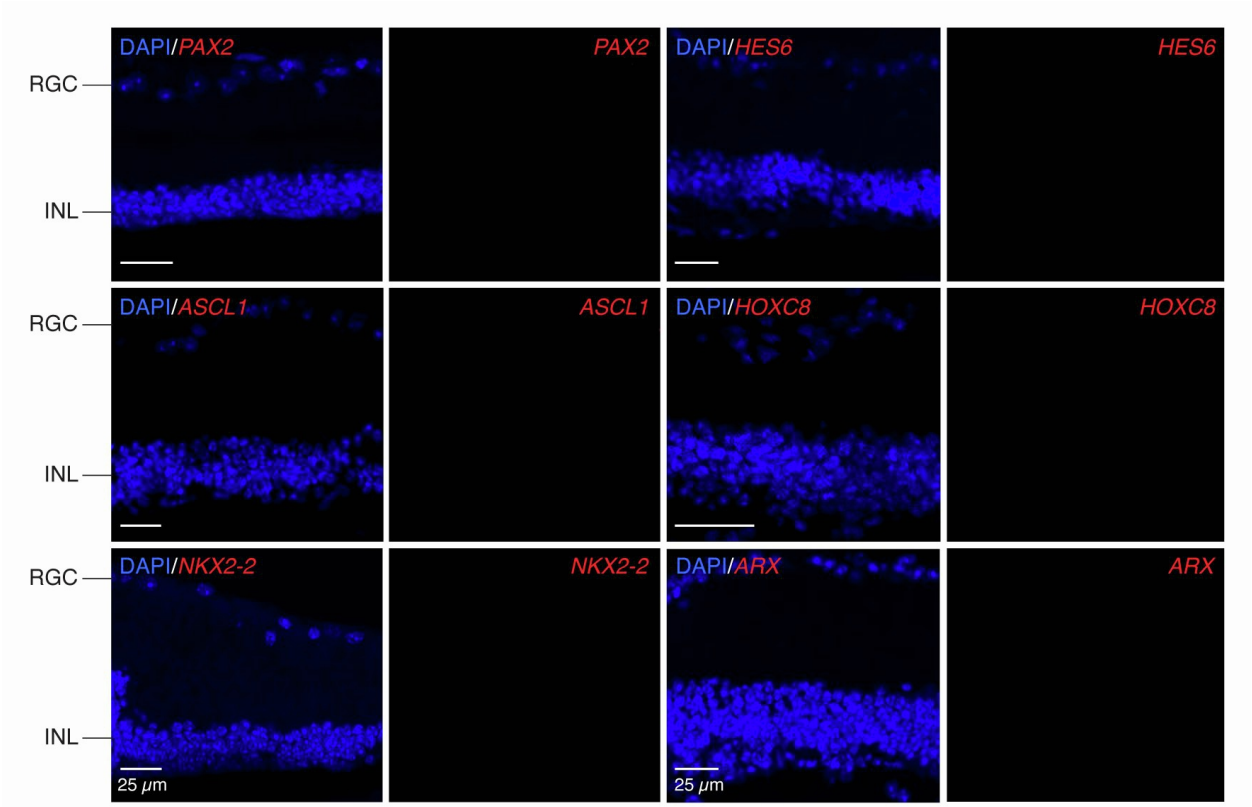

Fig. S4. RNAscope staining of human astrocyte and BSL on non-transplanted *Rd1/NS* control mice. Cryosections of non-transplanted *Rd1/NS* mice were stained with human probes of astrocyte (*PAX2*) and BSL cells (*HES6*, *ASCL1*, *HOXC8*, *NKX2-2*, *ARX*). None of these human genes were detected in non-transplanted *Rd1/NS* mice retinae. *Abbreviation: RGC: retinal ganglion cell layer; INL: inner nuclear layer.*

Supplemental Figure 5

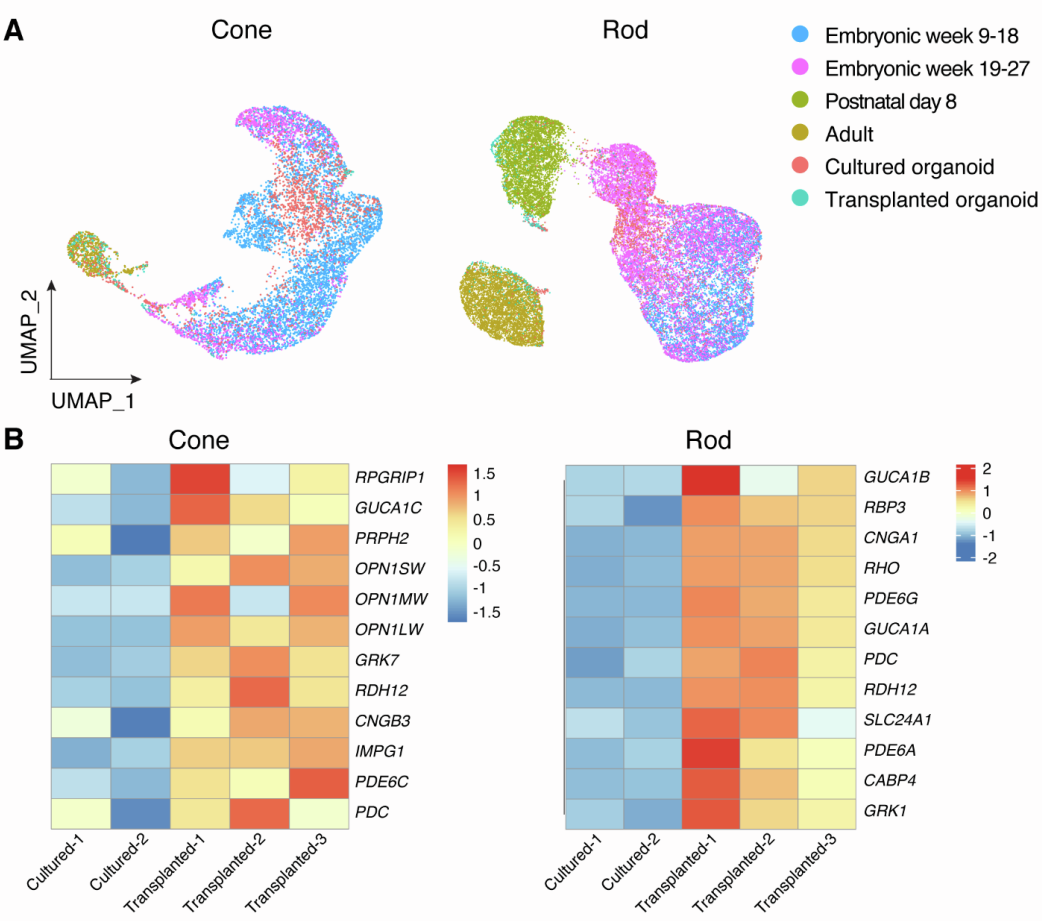

Fig. S5. Upregulation of cone and rod marker genes in transplanted retinal organoids. (A) UMAP plots showed cells colored by sample libraries, including human retina developmental datasets (cone: n = 7,654 cells, rod: n = 25,186 cells), cultured retinal organoids (cone: n =1,639 cells, rod: n=1,469 cells, collecting from two organoids in one batch), and transplanted retinal organoids (cone: n=210 cells, rod: n =504 cells, collecting from three transplanted eyes). **(B)** Heatmaps demonstrated the upregulation of marker genes specific for cone and rod photoreceptors in transplanted retinal organoids (including three independent replicates "Transplanted-1, Transplanted-2, Transplanted-3"), compared to cultured retinal organoids (including two independent replicates "Cultured-1, Cultured-2" from one batch).

Supplemental Figure 6

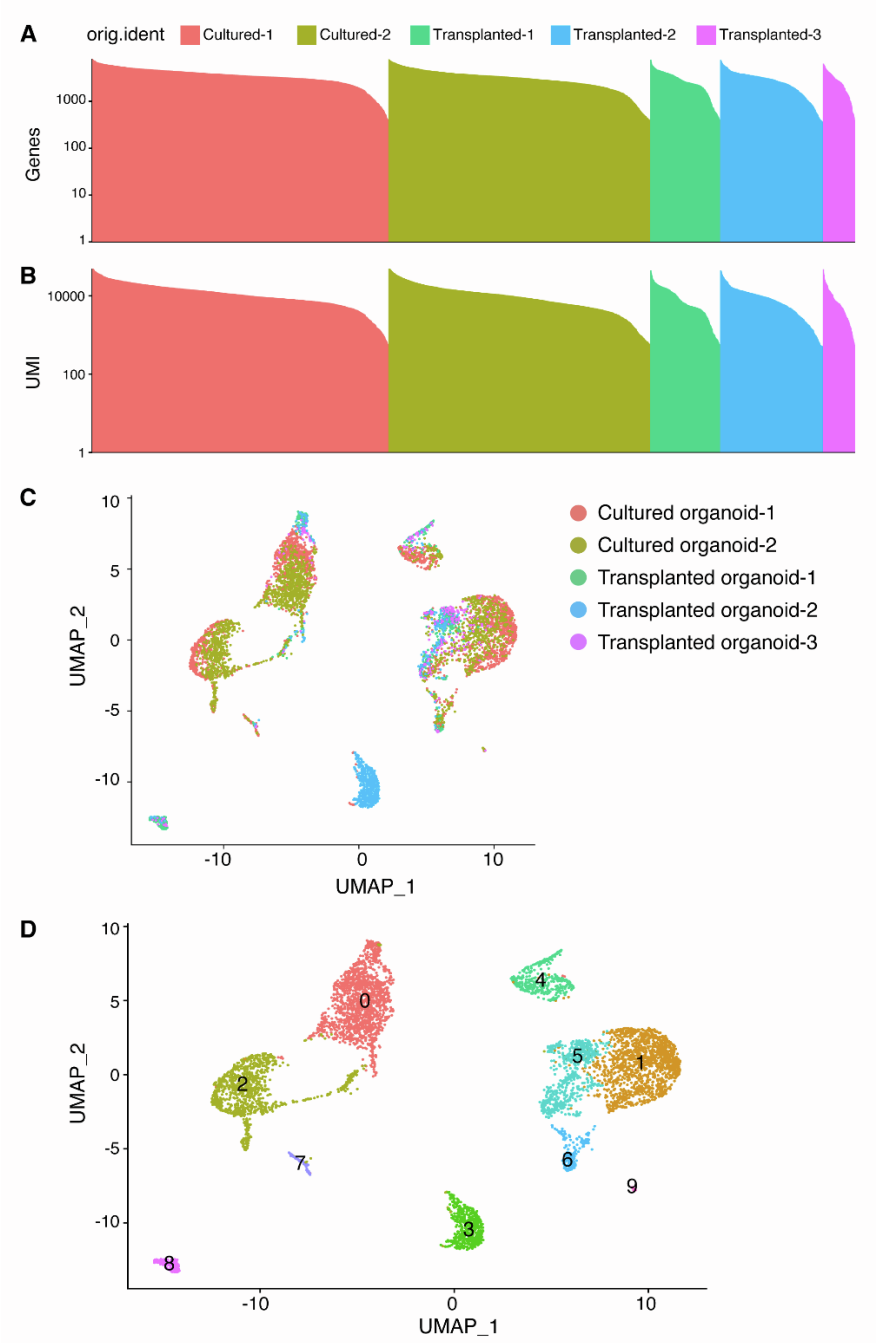

Fig. S6. Quality control of scRNA-seq data. (A) Number of genes and **(B)** unique molecular identifiers (UMI) per cell. Each bar is a cell and is colored by the sample library and ordered along the x-axis in descending order. **(C)** UMAP plot showing cells colored by sample library. **(D)** UMAP plot showing 10 (0-9) transcriptionally distinct cell clusters.

Supplemental Figure 7

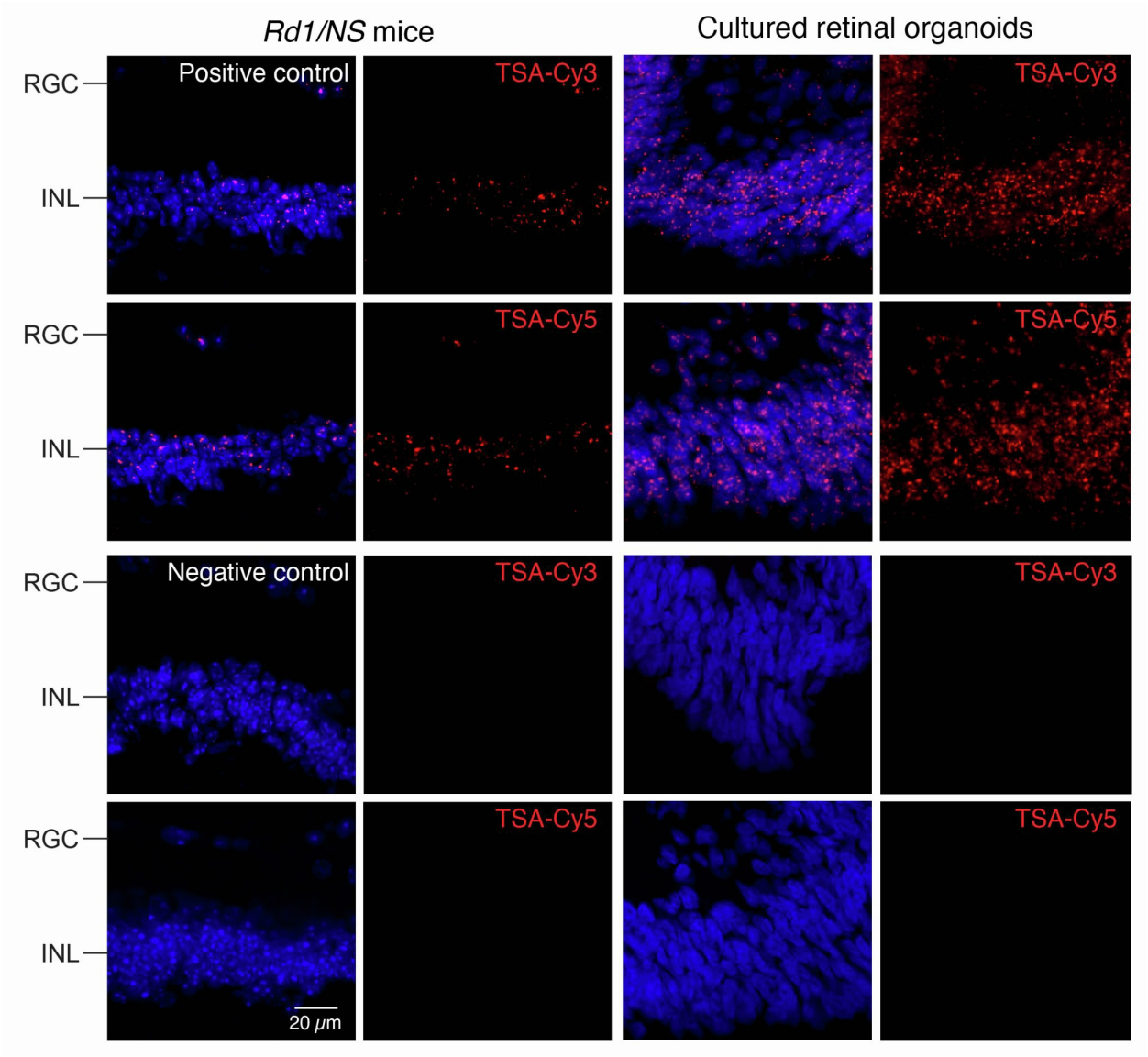

Fig. S7. RNAscope staining of positive and negative control probes. Cryosections of non-transplanted *Rd1/NS* mice and cultured retinal organoids were stained with 3-plex positive and negative control probes in combination with TSA-Cy3 or TSA-Cy5 fluorophores. Positive probes target common housekeeping genes *PPIB* (Cy3) and *POLR2A* (Cy5). Negative probe targets the bacterial dapB gene.

Table S1. BE6.2 media and long-term retina media (LTR) for Crx:tdTomato^{+} retinal organoids.

Reagent	Concentration	Source	Catalog Number
BE6.2 media			
DMEM	—	Gibco	11885084
B27 minus vitamin A	2%	Gibco	12587010
Glutamax	1%	Gibco	35050061
NEAA	1%	Gibco	11140050
Sodium pyruvate	1mM	Gibco	11360070
NaCl	0.87 mg/mL	Sigma-Aldrich	S9888
E6 supplement	**2.5%**		
Insulin	970 ug/mL	Roche	11376497001
Holo-transferrin	535 ug/mL	Sigma-Aldrich	T0665
L-ascorbic acid	3.20 mg/mL	Sigma-Aldrich	A8960
Sodium selenite	0.7 ug/mL	Sigma-Aldrich	S5261
long-term retina (LTR) media			
DMEM	—	Gibco	11885084
F12	25%	Gibco	11765062
B27	2%	Gibco	17504044
NEAA	1%	Gibco	11140050
Fetal bovine serum	10%	Gibco	16140071
Sodium pyruvate	1mM	Gibco	11360070
Glutamax	1%	Gibco	35050061
Taurine	1 mM	Sigma-Aldrich	T-8691

Table S2. Retinal organoid culturing media using hiPS cell line.

Reagent	Concentration	Source	Catalog Number
Neural Induction Media (NIM) (Day 3-Day 15)			
DMEM/F12 (1:1)	—	Life Technologies	11330-057
100x N2 Supplement	1% (v/v)	Life Technologies	17502-048
HEPARIN (stock as 1mg/mL in DMEM, 0.1%)	2 ug/mL	Sigma	H3149-100
100x MEM-NEAA	0.01	Life Technologies	11140050
Retinal Differentiation Media (RDM) (Day 16-Day 30)			
DMEM	—	Life Technologies	11330-057
F12	—	Life Technologies	11965
50x B27 (without Vit A)	1x	Life Technologies	11765
100x Antibiotic and Antimycotic	1x	Life Technologies	12587-010
100x MEM-NEAA	1x	Life Technologies	15240
RC2 (Day 30-Day 91)			
DMEM	----	Life Technologies	11965
F12	----	Life Technologies	11765
50x B27 (without Vit A)	1x	Life Technologies	12587010
100x Antibiotic and Antimycotic	1x	Life Technologies	15240
100x MEM-NEAA	1x	Life Technologies	11140050
FBS	10%	Gibco or Atlanta Biologicals	S11150
100x Glutamax	1x	Life Technologies	35050061
1000x Taurine (100mM)	100 uM	Sigma	T0625

Retinoic Acid (directly add RA to cells when changing media)	0.5-1 uM	Sigma-Aldrich	R2625
RC1 (>Day 91)			
DMEM/F12-Glutamax	----	Life Technologies	10565-018
100x N2 Supplement	1% (v/v)	Life Technologies	17502-048
100x Antibiotic and Antimycotic	1x	Life Technologies	15240
100x NEAA	1x	Life Technologies	11140050
FBS	10%	Atlanta Biologics	S11150
1000x Taurine (100mM)	100 uM	Sigma	T0625
Retinoic Acid (directly add RA to cells when changing media)	0.5 uM	Sigma-Aldrich	R2625

87

Table S3. Forward and reverse primer sequences used for mice genotyping.

Gene	F primer (5' to 3')	R primer (5' to 3')
Rd1 Wild type	ACTCTGTGGCCTCAAAGATACATC	TGCAGGTCACAGAATCATCATAACA
Rd1 Mutant	GGGTCTCCTCAGATTGATTGACTAC	GTCACTCTGTGGCCTCAAAGAT
NOD/Scid	TGTAACGGAAAAGAATTGGTATCCACA	GTTGGCCCCTGCTAACTTTCT

Table S4. Reagents used for RNAscope staining.

Reagents	Dilution	Source	Catalog Number
RNA probes			
PAX2-Hs	No dilution	Advanced Cell Diagnostics	442541
HES6-Hs	1:50	Advanced Cell Diagnostics	521301-C2
ASCL1-Hs	1:50	Advanced Cell Diagnostics	459721-C2
NKX2-2-Hs	No dilution	Advanced Cell Diagnostics	821401
HOXC8-Hs	No dilution	Advanced Cell Diagnostics	506531
ARX-Hs	1:50	Advanced Cell Diagnostics	486711-C2
VSX2-Hs	1:50	Advanced Cell Diagnostics	493031-C2
3-plex positive control-Mm	No dilution	Advanced Cell Diagnostics	320881
3-plex positive control-Hs	No dilution	Advanced Cell Diagnostics	320861
3-plex negative control	No dilution	Advanced Cell Diagnostics	320871
TSA-fluorophores			
TSA plus-Cy3	1:1500	AKOYA Biosciences	NEL744001KT
TSA plus-Cy5	1:1500	AKOYA Biosciences	NEL745001KT

Table S5. Antibodies used for RNAscope counterstaining and immunohistochemistry staining.

Reagents	Dilution	Source	Catalog Number
Primary antibodies			
Rabbit anti-RBPMS	1:500	MilliporeSigma	ABN1362
Mouse anti-NeuN	1:500	MilliporeSigma	MAB377
Mouse anti-Calbindin	1:500	Sigma-Aldrich	C9848
Goat anti-PKCα	1:200	R&D Systems	AF5340
Goat anti-SCGN	1:200	Thermo Fisher Scientific	PA5-47664
Rabbit anti-IBA1	1:250	Abcam	Ab178680
Rabbit anti-CD68	1:100	Abcam	Ab125212
Rabbit anti-Ki67	1:500	Thermo Fisher Scientific	MA5-14520
Rabbit anti-L/M-opsin	1:500	Kerafast	EDK101
Rabbit anti-S-opsin	1:500	MilliporeSigma	Ab5407
Rabbit anti-Rhodopsin	1:500	Abcam	Ab3424
Mouse anti-human nuclear antibody (HNA)	1:1000	MilliporeSigma	Mab1281
Sheep anti-Ki67	1:40	R&D Systems	AF7617
Rabbit anti-Ku80	1:50	Thermo Fisher Scientific	MA5-32212
Secondary antibodies			
Goat anti-Rabbit 488	1:500	Abcam	Ab150077
Goat anti-Mouse 488	1:500	Thermo Fisher Scientific	A-11001
Goat anti-Mouse 647	1:500	Thermo Fisher Scientific	A32728
Donkey anti-Goat 488	1:500	Abcam	Ab150129
Donkey anti-Sheep 647	1:200	Thermo Fisher Scientific	A-21448
Donkey anti-Rabbit 488	1:200	Thermo Fisher Scientific	A21206

Supplemental experimental procedures

Cell Lines

The use of human stem cells was approved by the Johns Hopkins ISCRO (ISCRO00000249). The H9 CRX:tdTomato human embryonic stem cell line (hESCs) was a kind gift from Dr. David M. Gamm (University of Wisconsin Hospitals, USA) and Dr. Donald J. Zack (Johns Hopkins University, USA). The hiPSC line derived from CD34+ cord blood is a commercially available cell line (A18945, Thermo Fisher Scientific)(Burridge et al., 2011). The use of human iPSCs for generation of retinal organoids in this study conforms to the University of Colorado Office of Regulatory Compliance. Stem cells were maintained in mTeSR1 (Stem Cell Technologies, Cambridge, MA, USA) on 1% (vol/vol) Matrigel-GFRTM (BD Biosciences, USA, No. 354230,) coated dishes and grown in a 37°C HERAcell 150i incubator at 10%CO2 and 5% O2 incubator (Thermo Fisher Scientific, MA, USA). Cells were passaged upon confluence (every 3-6 days) using Accutase (Sigma-Aldrich, MO, USA, No. SCR005) for 7–10 minutes, and dissociated into single cells. Cells in Accutase were added 1:2 to mTeSR1 plus 5 μM Blebbistatin (Bleb; B0560, Sigma), pelleted at 700 g for 5 minutes, and suspended in mTeSR1 plus Bleb and plated at 5,000 cells per well in a six-well plate. After 48 hours, cells were fed with mTeSR1 (without Bleb) every 24 hours until the next passage. To minimize cell stress, no antibiotics were used in RPMI (Gibco, USA) and supplement media (10% fetal bovine serum (FBS), 2.5% penicillin). Cells were maintained at 37°C and 5% CO2 and passaged every 3-4 days at ~1 x $10^{\wedge 5}$ – 2 x $10^{\wedge 6}$ cells/ml in uncoated flasks. Cells were routinely tested for mycoplasma using MycoAlert (Lonza, Switzerland, No. LT07).

Retinal organoid culturing

For H9 CRX:tdtomato^{+} retinal organoid culturing, the hESCs were dissociated in Accutase at 37°C for 12 min and seeded in 50 µl of mTeSR1 at 3,000 cells/well into 96-well ultra-low adhesion round bottom Lipidure coated plates (AMSBIO, MA, USA, No.51011610). Cells were placed in hypoxic conditions (10% CO2 and 5% O2) for 24 hours to enhance survival. Cells naturally aggregated by gravity over 24 hours. On day 1, cells were moved to normoxic conditions (5% CO2). On days 1- 3, 50 µl of BE6.2 media, **Table S1**) containing 3 µM Wnt inhibitor (IWR1e, EMD Millipore, MA, USA, No. 681669,) and 1% (v/v) Matrigel were added to each well. On days 4-9, 100 µl of media were removed from each well, and 100 µl of media were added. On days 4-5, BE6.2 media containing 3 µM Wnt inhibitor and 1% Matrigel was added. On days 6-7, BE6.2 media containing 1% Matrigel was added. On days 8-9, BE6.2 media containing 1% Matrigel and 100 nM Smoothened agonist (SAG, EMD Millipore, No. 566660) was added. On day 10, aggregates were transferred to 15 mL tubes, rinsed 3X in DMEM (Gibco, No. 11885084), and resuspended in BE6.2 with 100 nM SAG in untreated 10 cm polystyrene petri dishes. From this point on, media was changed every other day. Aggregates were monitored and manually separated if stuck together or to the bottom of the plate. On day 11, retinal vesicles were manually dissected using sharpened tungsten needles. After dissection, cells were transferred into 15 mL tubes and washed 2X with 5 mLs of DMEM. On days 14-17, long-term retina (LTR, **Table S1**) media with 100 nM SAG was added. On days 18-21, cells were maintained in LTR and washed 2X with 5 mLs of DMEM, before being transferred to new plates to wash off dead cells. To increase survival and differentiation, 1 µM all-trans retinoic acid (ATRA; R2625; Sigma) was added to LTR medium from days 22-138. 10 µM Gammasecretase inhibitor (DAPT, EMD Millipore, No. 565770) was added to LTR from days 28-42. Retinal organoids were grown at low density (10-20 per 10 cm dish) to reduce aggregation.

For the generation of retinal organoids from human iPS cells, a human induced pluripotent stem cell (hiPSC) line derived from $CD34^+$ cord blood was used for all experiments in this study (A18945, ThermoFisher Scientific) (Burridge *et al.*, 2011). Cell culture, retinal differentiation, and human retinal organoid formation were conducted as previously described (Zhong et al., 2014). A more detailed protocol of the methodology for generating retinal organoids was recently described (Aparicio-Domingo et al., 2023). Briefly, hiPSCs were maintained on Matrigel (growth-factor-reduced; BD Biosciences) coated plates. After 6 days in culture, hiPSC colonies were lifted and cultured as free-floating neural aggregates (NAs); this was established as Day 0 (D0) of differentiation. On D7, NAs were seeded onto Matrigel (growth-factor-reduced; BD Biosciences) coated dishes, and individual mechanical detachment of the NR and RPE domains was performed between D21 and D23. The culture media and reagents are listed in **Table S2.** Undifferentiated hiPSCs and derived retinal organoids were routinely tested for Mycoplasma contamination by PCR.

Animals

All animal experiments were carried out in accordance with the ARVO Statement for the Use of Animals in Ophthalmic and Vision Research. All procedures were approved by the Johns Hopkins University Animal Care and Use Committee (approval M016M17). The C3H/HeJ-*Pde6*$^{Rd1/Rd1}$ (referred to as *Rd1*), and NOD.Cg-*Prkdc*^{scid}/J (referred to as *NOD/Scid*) mice of either gender (aged 6 to 8 weeks) were obtained from Jackson Laboratory (Bar Harbor, ME, USA). All mice were housed in cages under a 12:12-hour light-dark cycle with water and food provided *ad libitum*.

Recipient mice

We created a recipient mouse model with immune-deficiency and retinal degeneration (referred to as *Rd1/NS*) by crossbreeding *Rd1* mice and *NOD/Scid* mice (aged 8 weeks). The breeding strategy was performed as previously reported (Wenzel et al., 2007). Genomic DNA of the third-generation

offspring was extracted from ear biopsies and genotyped by Transnetyx Tag Center (Cordova,TN, USA). Primers were listed in **Table S3**. Eyes of adult *Rd1/NS* mice (n=3) were collected to characterize photoreceptor degeneration using immunohistochemistry (IHC) staining, as previously reported (Liu et al., 2021). Flow cytometry was performed using spleen biopsies of adult *Rd1/NS* mice (n=3) to confirm the deficiency of T cells and B cells, as previously described (Hensel et al., 2019). Phenotyping data of *Rd1/NS* mice are shown in **Fig. S1**.

Preparation of donor cells

Donor retinal organoid cells (harvested as micro-dissected multilayered retinal fragments) were obtained from CRX:tdTomato^{+} hESC-derived retinal organoids (aged 134 days, n=4) and hiPSC derived retinal organoids (aged 150 days, n=3). The cultured human retinal organoids were imaged using a fluorescent microscope (Carl Zeiss, Jena, Germany). The images were used as a reference to isolate the retinal cluster from the donor retinal organoids. The isolated retinal organoids clusters were then cut into 1 × 1 mm$^{\wedge 2}$ or 1 × 2 mm$^{\wedge 2}$ microdissected fragments using a 27-gauge horizontal curved scissors (VitreQ, Kingston, NH, USA) under a dissection microscope. Donor cells were transplanted within two hours of isolation.

Transplantation of donor cells

Donor retinal organoid fragments were transplanted into the subretinal space of *Rd1/NS* mice (aged 6 to 8 weeks, n=16 eyes for hESC-derived retinal organoids, n=5 eyes for iPS-derived retinal organoids), as previously reported (Liu et al., 2020). Briefly, recipient mice were anesthetized by intraperitoneal injection of ketamine (100 mg/kg body weight) and xylazine hydrochloride (20 mg/kg body weight). Mouse pupils were dilated with 1% (wt/vol) tropicamide (Bausch & Lomb, Rochester, NY, USA). Mouse corneas were covered with Sodium Hyaluronate (Healon GV, Abbott Medical Optics Inc. CA, USA) and cover glasses (Deckglaser, USA) to facilitate

transpupillary visualization. The donor retinal organoid fragments were loaded into the bevel of a 26G microneedle with the photoreceptor side facing down, gently aspirated into the attached micro-syringe (Hamilton, Reno, NV, USA), then tangentially injected into the subretinal space through the sclera of the recipient mice. Successful injection was verified by direct visualization through the dilated pupil of the recipient under the surgical microscope (Leica, Wetzlar, Germany).

Single cell RNA sequencing

Single cell RNA sequencing (scRNA-seq) was performed on dissociated cells from transplanted and cultured CRX:tdTomato^{+} retinal organoids using the Chromium platform (10X Genomics). Briefly, retinal organoid cells were dissociated into a single cell suspension using the Papain Dissociation System (Worthington) for 60 minutes at 37°C, with gentle mixing every 5 minutes, before stopping the reaction using ovomucoid protease inhibitors. Cells were centrifuged and resuspended in ice-cold PBS containing 0.04% bovine serum albumin (BSA) and 0.5 U/µl RNase inhibitor and were filtered through a 40-µm Flowmi cell strainer (Bel-Art SP). Cell counts and viability were assessed by Trypan blue staining before loading 6000 cells on a Chromium Single Cell system using Next GEM 3' reagent v3.1 kits. Libraries were pooled and sequenced on Illumina NextSeq 500 with ~50,000 reads per cell. The Cell Ranger 4 (10X Genomics) pipeline was used to process the raw sequencing reads for demultiplexing. Since the starting material used to generate the library consisted of human and mouse cells, reads were aligned to a hybrid GRCm38 mouse and GRCh38 human reference genome. Cell barcodes that had most of their reads mapped to GRCm38 mouse genes were considered to be of mouse origin and excluded. The remaining cellular barcode-associated reads were re-mapped to the GRCh38 human reference genome and a cell-by-gene count matrix was generated for downstream analysis. In this study, only the human cells were ultimately analyzed. The generated cell-by-gene count matrices were

analyzed using the Seurat ver3 R package (Stuart et al., 2019). We filtered out cells that had UMIs less than 300 or greater than 50000 and with a mitochondrial fraction of greater than 20%. Doublets were identified and removed using the DoubletFinder R package (McGinnis et al., 2019). Log-normalization, scaling, UMAP dimensional reduction and clustering were performed using the standard Seurat pipeline. Quality control of scRNA-seq data were shown in **Fig. S6**. Major retinal cell types were identified using previously identified cell type markers (Hoang et al., 2020). Enriched genes from the brain/spinal-like cell cluster were compared to the ASCOT (Ling et al., 2020) gene expression summaries of public RNA-Seq data to determine its classification. Differential gene tests were performed by Seurat's *FindMarkers* function using the Wilcoxon rank sum test with default parameters (Stuart *et al.*, 2019). Hierarchical clustering was used to group the differentially expressed genes. The UCell R package (Andreatta and Carmona, 2021) was used to calculate the migration potential score or the proliferation score (**data files S1, S2**). The gene sets were constructed by identifying enriched genes within the gene ontology terms cell migration and cell motility for the migration potential score and cell division for the proliferation score respectively. The Seurat integration functions (*SelectIntegrationFeatures*, *FindIntegrationAnchors* and *IntegrateData*) were used to integrate the organoid data onto the human retinal developmental dataset (Lu et al., 2020). Monocle 3 (Cao et al., 2019) was used to perform pseudotime analysis and identify trajectory routes within the data.

Histology

Four and a half months post-transplantation, the recipient mice were sacrificed with over-dose anesthesia and pre-fixed by heart-perfusion with 4% paraformaldehyde (PFA) (Electron Microscopy Sciences, Hatfield, PA, USA) in PBS. Eyes were gently removed, post-fixed in 4% PFA/PBS for one hour at room temperature (RT), and dehydrated in a sucrose gradient (10%, 20%,

30%), then blocked in optimal cutting temperature compound (Sakura Finetek, Torrance, CA, USA). Cultured retinal organoids were fixed in 4% PFA at RT for 15 minutes (min), dehydrated in gradient sucrose (10%, 20%, 30%), and blocked in the OCT compound. OCT-blocked recipient mouse eyes and cultured retinal organoids were cut into 7-10 μm thick cryosections using a microtome (CM 1850; Leica) for histological staining.

RNAscope and IHC counter-staining was performed according to the manufacturer's protocol (Advanced Cell Diagnostics (ACD), see Protocol #MK 51-150, Appendix D.). Briefly, cryosections of recipient mice eyes and cultured retinal organoids were rinsed with PBS, baked in a HybEZTM oven (ACD, USA) for 30 min at 60°C, and post-fixed in pre-chilled 4% PFA in PBS for 15 min at 4°C. Slides were dehydrated in gradient ethanol (50%, 70%, 100%), treated with hydrogen peroxide (10 min at RT), then subjected to target retrieval using the Co-detection Target Retrieval solution (ACD, Cat. No. 323180) at 98-102°C for 5 min. After rinsing in distilled water (2 min x 2) and PBS-T (5 min x 1), the slides were incubated with diluted primary antibody at 4°C overnight. On day 2, slides were post-fixed with 4% PFA for 30 min at RT, treated with protease III at 40°C for 30min, and subjected to RNAscope staining using the RNAscope Multiplex Fluorescent V2 assay according to the manufacturer's protocol (ACD, RNAscope USM-323100, see "fixed-frozen tissue sample protocol"). Briefly, RNA probe hybridization was performed with the HybEZTM oven for two hours at 40°C. Slides were then assigned for three series of amplification, fluorochromes combination, and HRP blocking. After the RNAscope procedure, slides were incubated with secondary antibody at RT for one hour, counter stained with DAPI, and mounted with Prolong Diamond (Life Technology, Carlsbad, CA, USA). The RNA probes, fluorophores used were listed in **Table S4**. The primary and secondary antibodies used for IHC

counter staining were listed in **Table S5**. Negative and positive multiplex control probes staining were run in parallel with the target probes following the same protocol (data shown in **Fig. S7**).

IHC staining was performed as previously described (Liu *et al.*, 2020). Briefly, cryosections of transplanted *Rd1/NS* mice and cultured retinal organoids were rinsed with PBS (5 min x 1), permeabilized, and blocked with a mixture of 0.1% Triton-X100 and 5% goat serum in PBS for one hour at RT. The slides were rinsed in PBS (5 min x 3), incubated with primary antibodies at 4°C overnight, incubated with secondary antibodies at RT for one hour, then counter stained with DAPI and mounted using ProLong Diamond mounting media. The primary antibodies and secondary antibodies used here were listed in **Table S5**.

Quantification of donor cell migration of recipient retina

For migratory distance quantification of transplanted retinal organoid cells, retinal sections from recipient mice were stained with human nuclear specific antibodies HNA (Sigma-Aldrich, MO, USA) or Ku80 (Thermo Fisher Scientific, MA, USA). Tile scan images were collected using Confocal LSM 880 (Zeiss, Oberkochen, Germany) for distance quantification. The migratory distance of transplanted retinal organoids was defined as the shortest distance between the migratory cells and the nearest graft edge (i.e., the graft-left migratory cells to the left endpoint of the graft; the graft-right migratory cells to the right endpoint of the graft). We used a mathematical method to facilitate distance quantification. Specifically, the graft edge was defined as a "starting point" and the migratory cells in different retinal laminae (RGC, IPL, INL, RPE/C) were manually targeted, both processed with the "Cell Counter" plugin in ImageJ. The cell coordinates were automatically collected to quantify the X and Y axial distances of individual cells by the Cell Counter. The axial distance of the graft edge (starting point) was referred to as "X_{start}" and "Y_{start}". The axial distance of the migratory cells was referred to as "$X_{migratory}$" and "$Y_{migratory}$". The

migratory distance was computed in R platform (see supplementary **coding file S1**) following the formula:

$$Migrating\ distance\ = \sqrt{(X_{start} - X_{migratory})^2\ +\ (Y_{start} - Y_{migratory})^2}$$

The unit of the migrating distance was converted from pixel to micron according to the image scale.

For cell quantification, the number of positively stained cells was manually counted using the "Cell Counter" plugin in ImageJ. The representative pre-synapse graphs of the transplanted and cultured retinal organoids were drawn by Imaris software (Version 9.5.0, Bitplane AG, Zurich, Switzerland).

Electrophysiology

The electrophysiological recording was performed on the transplanted CRX:tdTomato$^+$ photoreceptors eight months post-transplantation to measure their physiological properties. We were able to test only one recipient mouse (the second recipient mouse died before the assay during the long-term observation). The recipient's eyes were gently pulled out from the recipient mouse and put in Ames' medium (Sigma No. A1420). Retinas with transplanted retinal organoids were dissected by removing the corneas and lens under infrared light, attached to a piece of filter, sectioned into 200μm slices, and transferred to a recording chamber. The CRX:tdTomato$^+$ photoreceptors of the transplanted retinal organoids were targeted under an epifluorescence microscope for consequent whole-cell patch-clamp recording. Fluorescent signal was imaged by a Nikon CCD camera with data acquisition synchronized with a 20-ms flash of epi-fluorescence excitation light. The total exposure time to excitation light before recording was <500 ms. During recording, retina was perfused with Ames' medium bubbled with 95% O_2/5% CO_2. Patch electrodes (5-7 MΩ) were pulled from borosilicate capillaries (GC150-10, Harvard Apparatus) and

filled with an internal solution containing typically (in mM): 120 K-gluconate, 5 NaCl, 4 KCl, 10 HEPES, 2 EGTA, 4 ATP-Mg, 0.3 GTP-Na_2, and 7 Phosphocreatine-Tris, with pH adjusted to 7.3 with KOH. Whole-cell patch-clamp recording was made at 30–32^{o}C with an Axon Instruments Multiclamp 700B amplifier. Series resistance of patch electrodes was 10–30 MΩ. Liquid-junction potential (measured to be -13 mV) has been corrected. In voltage-clamp mode, recorded cells were held at -40 mV, followed by voltage steps of 100-ms (-70 mV to -10 mV). All procedures were carried out in the darkroom to avoid photoreceptor bleaching.

Statistical analysis

Quantitative histology data were analyzed using two-way ANOVA. Sidak's test or Tukey's test was adopted for multiple comparisons (two-tailed). Independent T-test or Mann-Whitney U test was used for two variants comparison. Statistical analysis was carried out using SPSS software (version 25, IL, USA). $p < 0.05$ was taken to be significant. Statistical data were presented as mean ± SD. Graphs were drawn with GraphPad Prism software (version 8, CA, USA). Schematics were created with BioRender.com (agreement number QH23QWJX12, KY23QWKEPB).

Supplemental References

Andreatta, M., and Carmona, S.J. (2021). UCell: Robust and scalable single-cell gene signature scoring. Comput Struct Biotechnol J *19*, 3796-3798. 10.1016/j.csbj.2021.06.043.

Aparicio-Domingo, S., Flores-Bellver, M., Cobb, H., Li, K.V., Conrad, B., Chen, C., Brzezinski, J.A., and Canto-Soler, M.V. (2023). Generation of Three-Dimensional Retinal Tissue with Physiologically Competent, Light-Sensitive Photoreceptors from Human-Induced Pluripotent Stem Cells. In Brain Organoid Research, J. Gopalakrishnan, ed. (Springer US), pp. 99-119. 10.1007/978-1-0716-2720-4_6.

Burridge, P.W., Thompson, S., Millrod, M.A., Weinberg, S., Yuan, X., Peters, A., Mahairaki, V., Koliatsos, V.E., Tung, L., and Zambidis, E.T. (2011). A universal system for highly efficient cardiac differentiation of human induced pluripotent stem cells that eliminates interline variability. PLoS One *6*, e18293. 10.1371/journal.pone.0018293.

Cao, J., Spielmann, M., Qiu, X., Huang, X., Ibrahim, D.M., Hill, A.J., Zhang, F., Mundlos, S., Christiansen, L., Steemers, F.J., et al. (2019). The single-cell transcriptional landscape of mammalian organogenesis. Nature *566*, 496-502. 10.1038/s41586-019-0969-x.

Hensel, J.A., Khattar, V., Ashton, R., and Ponnazhagan, S. (2019). Characterization of immune cell subtypes in three commonly used mouse strains reveals gender and strain-specific variations. Lab. Invest. *99*, 93-106. 10.1038/s41374-018-0137-1.

Hoang, T., Wang, J., Boyd, P., Wang, F., Santiago, C., Jiang, L., Yoo, S., Lahne, M., Todd, L.J., Jia, M., et al. (2020). Gene regulatory networks controlling vertebrate retinal regeneration. Science (New York, N.Y.) *370*. 10.1126/science.abb8598.

Ling, J.P., Wilks, C., Charles, R., Leavey, P.J., Ghosh, D., Jiang, L., Santiago, C.P., Pang, B., Venkataraman, A., Clark, B.S., et al. (2020). ASCOT identifies key regulators of neuronal subtype-specific splicing. Nat Commun *11*, 137. 10.1038/s41467-019-14020-5.

Liu, Y.V., Sodhi, S.K., Xue, G., Teng, D., Agakishiev, D., McNally, M.M., Harris-Bookman, S., McBride, C., Konar, G.J., and Singh, M.S. (2020). Quantifiable in vivo imaging biomarkers of retinal regeneration by photoreceptor cell transplantation. Transl. Vis. Sci. Technol. *9*, 5. 10.1167/tvst.9.7.5.

Liu, Y.V., Teng, D., Konar, G.J., Agakishiev, D., Biggs-Garcia, A., Harris-Bookman, S., McNally, M.M., Garzon, C., Sastry, S., and Singh, M.S. (2021). Characterization and allogeneic transplantation of a novel transgenic cone-rich donor mouse line. Exp. Eye Res. *210*, 108715. 10.1016/j.exer.2021.108715.

Lu, Y., Shiau, F., Yi, W., Lu, S., Wu, Q., Pearson, J.D., Kallman, A., Zhong, S., Hoang, T., Zuo, Z., et al. (2020). Single-cell analysis of human retina identifies evolutionarily conserved and species-specific mechanisms controlling development. Dev. Cell *53*, 473-491.e479. 10.1016/j.devcel.2020.04.009.

McGinnis, C.S., Murrow, L.M., and Gartner, Z.J. (2019). DoubletFinder: Doublet Detection in Single-Cell RNA Sequencing Data Using Artificial Nearest Neighbors. Cell Syst *8*, 329-337 e324. 10.1016/j.cels.2019.03.003.

Stuart, T., Butler, A., Hoffman, P., Hafemeister, C., Papalexi, E., Mauck, W.M., 3rd, Hao, Y., Stoeckius, M., Smibert, P., and Satija, R. (2019). Comprehensive Integration of Single-Cell Data. Cell *177*, 1888-1902 e1821. 10.1016/j.cell.2019.05.031.

Wenzel, A., von Lintig, J., Oberhauser, V., Tanimoto, N., Grimm, C., and Seeliger, M.W. (2007). RPE65 is essential for the function of cone photoreceptors in NRL-deficient mice. Invest. Ophthalmol. Vis. Sci. *48*, 534-542. 10.1167/iovs.06-0652.

Zhong, X., Gutierrez, C., Xue, T., Hampton, C., Vergara, M.N., Cao, L.H., Peters, A., Park, T.S., Zambidis, E.T., Meyer, J.S., et al. (2014). Generation of three-dimensional retinal tissue with functional photoreceptors from human iPSCs. Nat Commun *5*, 4047. 10.1038/ncomms5047.

Supplemental coding file S1

R coding algorithms for migrating distance quantification

```
library(data.table)
library(plyr)

##############################################################################
#
# Extract the X,Y coordinate of migrated cells, and generate subsequent distance data presented in
Table 1
#
##############################################################################

#---> Extracting data exported from ImageJ

common_path = "~/Desktop/cell invasion/Processed_Image"

files_to_read = list.files(
  path = common_path,        # directory to search within
  pattern = ".*(Rd1-NS).*csv$", # regex pattern
  recursive = TRUE,          # search subdirectories
  full.names = TRUE          # return the full path
)

#---> Hypothetical Researcher has 37 retina slides to quantify
#     and wants to localize 5 cell types per retina slides. So that's
#     37 rows and 6 columns (including cell id) in the data list

data_lst = lapply(files_to_read, read.csv)  # read all the matching files
celltype_summary = data.frame(matrix(ncol = 6, nrow = 37))
colnames (celltype_summary) <- c("File_name", "Type_1", "Type_2", "Type_3", "Type_4",
"Type_5")

#---> Calculating the distance from starting point for each cell
#     categorized by cell types

for (i in 1:length(data_lst)){
  data_lst[[i]]$Address <- rep(files_to_read[i],nrow(data_lst[[i]]))
```

```
  File_Name <-  files_to_read[i]
  Type_1 <- sum(data_lst[[i]]$Type == 1)
  Type_2 <- sum(data_lst[[i]]$Type == 2)
  Type_3 <- sum(data_lst[[i]]$Type == 3)
  Type_4 <- sum(data_lst[[i]]$Type == 4)
  Type_5 <- sum(data_lst[[i]]$Type == 5)
  celltype_summary[i,1:6] = c(File_Name, Type_1, Type_2, Type_3, Type_4, Type_5)
  print(c(File_Name, Type_1, Type_2, Type_3, Type_4, Type_5))
  for (j in 1:nrow(data_lst[[i]])){
  data_lst[[i]][j,"Z.µm."]=sqrt(( data_lst[[i]][j,"X.µm."]- data_lst[[i]][1,"X.µm."])^2 +
                                ( data_lst[[i]][j,"Y.µm."]- data_lst[[i]][1,"Y.µm."])^2) #distance calculation
  }
}

#---> Exporting analyzed invasion distance summary

dat1<-ldply(data_lst)

write.table(as.data.frame(dat1),file="Detialed_Result.csv", quote=F,sep=",",row.names=F)
write.table(as.data.frame(celltype_summary),file="Celltype_Summary.csv",
quote=F,sep=",",row.names=F)
```